

REPORT DOCUMENTATION PAGE

*Form Approved
OMB No. 0704-0188*

Public reporting burden for this collection of information is estimated to average 1 hour per response, including the time for reviewing instructions, searching existing data sources, gathering and maintaining the data needed, and completing and reviewing this collection of information. Send comments regarding this burden estimate or any other aspect of this collection of information, including suggestions for reducing this burden to Department of Defense, Washington Headquarters Services, Directorate for Information Operations and Reports (0704-0188), 1215 Jefferson Davis Highway, Suite 1204, Arlington, VA 22202-4302. Respondents should be aware that notwithstanding any other provision of law, no person shall be subject to any penalty for failing to comply with a collection of information if it does not display a currently valid OMB control number. **PLEASE DO NOT RETURN YOUR FORM TO THE ABOVE ADDRESS.**

| | | | | | |
|---|------------------------------------|--|--|--|---|
| 1. REPORT DATE (DD-MM-YYYY) July 2015 | | 2. REPORT TYPE Technical Paper | | 3. DATES COVERED (From - To) July 2015-July 2015 | |
| 4. TITLE AND SUBTITLE Simulation of Rocket Kerosene Flowing in an Electrically Heated Experimental Rig | | | | 5a. CONTRACT NUMBER In-House | |
| | | | | 5b. GRANT NUMBER | |
| | | | | 5c. PROGRAM ELEMENT NUMBER | |
| 6. AUTHOR(S) Ananda Himansu, Matt Billingsley, Nick Keim, Ben Hill-Lam, Claire Wilhelm | | | | 5d. PROJECT NUMBER | |
| | | | | 5e. TASK NUMBER | |
| | | | | 5f. WORK UNIT NUMBER Q0A4 | |
| 7. PERFORMING ORGANIZATION NAME(S) AND ADDRESS(ES) Air Force Research Laboratory (AFMC) AFRL/RQRC 10 E. Saturn Blvd. Edwards AFB, CA 93524-7680 | | | | 8. PERFORMING ORGANIZATION REPORT NO. | |
| 9. SPONSORING / MONITORING AGENCY NAME(S) AND ADDRESS(ES) Air Force Research Laboratory (AFMC) AFRL/RQR 5 Pollux Drive Edwards AFB CA 93524-7048 | | | | 10. SPONSOR/MONITOR'S ACRONYM(S) | |
| | | | | 11. SPONSOR/MONITOR'S REPORT NUMBER(S) AFRL-RQ-ED-TP-2015-283 | |
| 12. DISTRIBUTION / AVAILABILITY STATEMENT Distribution A: Approved for Public Release; Distribution Unlimited. | | | | | |
| 13. SUPPLEMENTARY NOTES Technical Paper and Presentation presented at AIAA Propulsion and Energy Forum; Orlando, FL; 2015 July 27-29. PA#15397. | | | | | |
| 14. ABSTRACT A model is developed of the steady three-dimensional combined flow of fluid, heat and electricity in an experimental apparatus designed to test fuel thermal stability. A numerical simulation is performed for the purposes of model validation and assessment of the detailed thermal characteristics of the apparatus. Conjugate heat transfer and electric current flow of rocket-grade kerosene (RP-2) flowing in an electrically heated tube is simulated. The model and boundary conditions are selected so as to simulate an experimental case reported in the fuel thermal stability literature. The model includes steady, incompressible, variable-density turbulent flow inside the tube, thermally coupled with steady heat conduction, and electric current flow in the solid copper apparatus. Temperature dependence of fluid and solid thermodynamic and transport properties is included in the model. The tube inner wall surface roughness is adjusted in order to match the cooling efficacy of the fuel in the simulation with that observed in the experiment. The simulation predicts an RP-2 temperature rise in agreement with experiment, and a tube wall thermal state largely in agreement with experiment. The simulation results are used to identify regions of temperature, current flux density, and Joule heating concentration in the experimental apparatus. The predicted tube wall temperatures at each end of the heated portion of the tube are significantly less than the experimentally observed values. The predicted temperatures of the thermal chokes contacting the tube are considerably less than the experimentally observed values. The conclusion is drawn that an un-modeled thermal resistance or resistive heating source is present in the experiment. | | | | | |
| 15. SUBJECT TERMS | | | | | |
| 16. SECURITY CLASSIFICATION OF: | | | 17. LIMITATION OF ABSTRACT SAR | 18. NUMBER OF PAGES 47 | 19a. NAME OF RESPONSIBLE PERSON Matthew Billingsley |
| a. REPORT Unclassified | b. ABSTRACT Unclassified | c. THIS PAGE Unclassified | | | 19b. TELEPHONE NO (include area code) 661-275-5885 |

Simulation of Rocket-Grade Kerosene Flowing in an Electrically Heated Experimental Apparatus

Ananda Himansu¹ and Matthew C. Billingsley²

Air Force Research Laboratory, Edwards AFB, California, 93524

Nicholas S. Keim³, Ben Hill-Lam⁴, and Claire Wilhelm⁵

Center for Aerospace-Defense Research and Engineering (CADRE)

The Johns Hopkins University, Columbia, Maryland, 21044

A model is developed of the steady three-dimensional combined flow of fluid, heat and electricity in an experimental apparatus designed to test fuel thermal stability. A numerical simulation is performed for the purposes of model validation and assessment of the detailed thermal characteristics of the apparatus. Conjugate heat transfer and electric current flow of rocket-grade kerosene (RP-2) flowing in an electrically heated tube is simulated. The model and boundary conditions are selected so as to simulate an experimental case reported in the fuel thermal stability literature. The model includes steady, incompressible, variable-density turbulent flow inside the tube, thermally coupled with steady heat conduction, and electric current flow in the solid copper apparatus. Temperature dependence of fluid and solid thermodynamic and transport properties is included in the model. The tube inner wall surface roughness is adjusted in order to match the cooling efficacy of the fuel in the simulation with that observed in the experiment. The simulation predicts an RP-2 temperature rise in agreement with experiment, and a tube wall thermal state largely in agreement with experiment. The simulation results are used to identify regions of temperature, current flux density, and Joule heating concentration in the experimental apparatus. The predicted tube wall temperatures at each end of the heated portion of the tube are significantly less than the experimentally observed values. The predicted temperatures of the thermal chokes contacting the tube are considerably less than the experimentally observed values. The conclusion is drawn that an un-modeled thermal resistance or resistive heating source is present in the experiment.

Nomenclature

| | |
|-----------|--|
| J | = electrical resistive heating power density |
| V | = electric field potential |
| σ | = electrical conductivity |
| \vec{e} | = electric field strength |
| \vec{j} | = electric current flux density |

I. Introduction

A key technology in the thermal management of liquid rocket engines and hypersonic aircraft is in-wall regenerative fuel cooling. In this technology, cool fuel from the fuel tank is pumped through cooling channels

Distribution A: Authorized for public release, distribution unlimited.

¹ Aerospace Engineer, Combustion Devices Branch, AFRL, Edwards AFB, CA 93524, Member, AIAA.

² Mechanical Engineer, Combustion Devices Branch, AFRL, Edwards AFB, CA 93524, Member, AIAA.

³ Research Engineer, CADRE, the Johns Hopkins University, Columbia, MD 21044, Member, AIAA.

⁴ Research Engineer, CADRE, the Johns Hopkins University, Columbia, MD 21044, Member, AIAA.

⁵ Research Engineer, CADRE, the Johns Hopkins University, Columbia, MD 21044, Member, AIAA.

embedded in the hot wall which requires cooling. In rocket engines, this wall is the wall of the combustion chamber or nozzle, and is exposed to very hot gaseous combustion products on one side. Through heat exchange, the fuel keeps the wall at a safe operating temperature.

With rocket engine designers pushing the envelope on specific impulse, fuels are being pushed past previous cooling performance limits. When hydrocarbon fuels are involved, the most severe limitation on cooling performance is the thermal stability limit of the fuel, the temperature above which the fuel will undergo significant pyrolysis and which will lead to carbonaceous channel wall deposits that will greatly reduce the cooling capacity of the fuel channels.

Chemists and engineers are formulating a great many advanced hydrocarbon fuels that are intended to have higher thermal stability limits than currently used rocket hydrocarbon fuels. There exists a need to rapidly and cost-effectively test the thermal stability of a large number of prepared formulations. The Compact Rapid Assessment of Fuel Thermal Integrity (CRAFTI) experimental apparatus installed at CPIAC is aimed at advanced fuels testing. The background, design and functional verification of the apparatus will be described in detail in future papers. The experiment involves flowing the fuel to be tested through an electrically heated tube with pressures and heat fluxes simulative of rocket engine coolant channels. The thermal stability limit is assessed by measuring the carbon deposit formation rate. The experiment is aimed at developing a new standardized thermal stability test.

The rocket propulsion division of AFRL has ongoing experimental and modeling research into advanced regenerative cooling arrangements. Model development and validation is a part of this research thrust. In previous work, the present authors simulated multiple design variants of an earlier iteration of the CRAFTI apparatus. In that work, only heat conduction in the solid portion of the rig was simulated in detail. The electrical heating was treated in a lumped fashion, and the convection from the tube wall to the fuel was treated with a convective boundary condition. That analysis showed that those designs were prone to failure by overheating of the copper busbars supplying electricity to the tube.

In the present study, the functioning of a revised design of the CRAFTI apparatus is analyzed in more detail than before. The conjugate heat transfer simulation, which treats both solid heat conduction and fluid convection in a coupled manner, is implemented with higher fidelity, and is coupled with a higher fidelity simulation of the electric current flow. The goals of this effort are to gain deeper understanding of the functioning of the apparatus, and to identify any areas where the robustness or effectiveness of the apparatus may be improved. The longer term goals are to develop and validate models capable of assessing the thermal stability of hydrocarbon fuels, and of being used to design regenerative cooling systems. In the present study, a simulation is performed of an experimental case that will be fully reported in upcoming publications. The case involves no deposit formation.

II. CRAFTI Apparatus Operation, Test Conditions and Simulation Boundary Conditions

The geometry of the principal portion of the CRAFTI apparatus is shown in Figure 1. The test article is a straight tube of small circular cross-section made of C10100 OFE copper. Tubes of differing inner diameters are available for tests. However, the tube involved in the test case that we simulate here has an inner diameter of 0.036 in. and an outer diameter of 0.125 in. The tube is electrically heated by an electric potential difference (voltage) from power supplies connected to the tube via the inlet (lower) and outlet (upper) busbars seen in the figure. The applied voltage causes a continuous current to flow along the tube wall against its electrical resistance. This results in resistive or so-called Joule heating of the portion of the tube wall between the two busbars. The heated length of the tube is 4 in. The tube is continuously cooled by flowing the hydrocarbon fuel whose thermal stability is being tested through the tube. In the current case, the fuel is RP-2. The present iteration on the CRAFTI apparatus design incorporates a thermal “choke”, of which there is one between each busbar and the tube. The choke, together with a cap, acts as a clamp to hold the tube at each busbar with the aid of stainless steel bolts that press the cap and choke to the busbar. These details are seen in views of the simulation mesh in Figures 7 and 8. The chokes have a much smaller cross-sectional area than the busbars, “choking” the electric current and the heat flux, and therefore undergo significant Joule heating while the busbars stay relatively cool because of their low electrical resistance. This design raises the choke temperature to roughly the same as the tube temperature and prevents the heat loss from the tube that would have taken place if the tube were directly in contact with the cooler busbar. This provides a more sharply defined uniform heat generation profile over the heated length of the tube. The experiment is designed to ideally provide a heat flux to the fuel that is uniform along the heated tube length. All solid parts are made of copper, except for the bolts which are made of stainless steel. The apparatus is operated in a vacuum chamber, so that there are no convective heat losses to the environment.

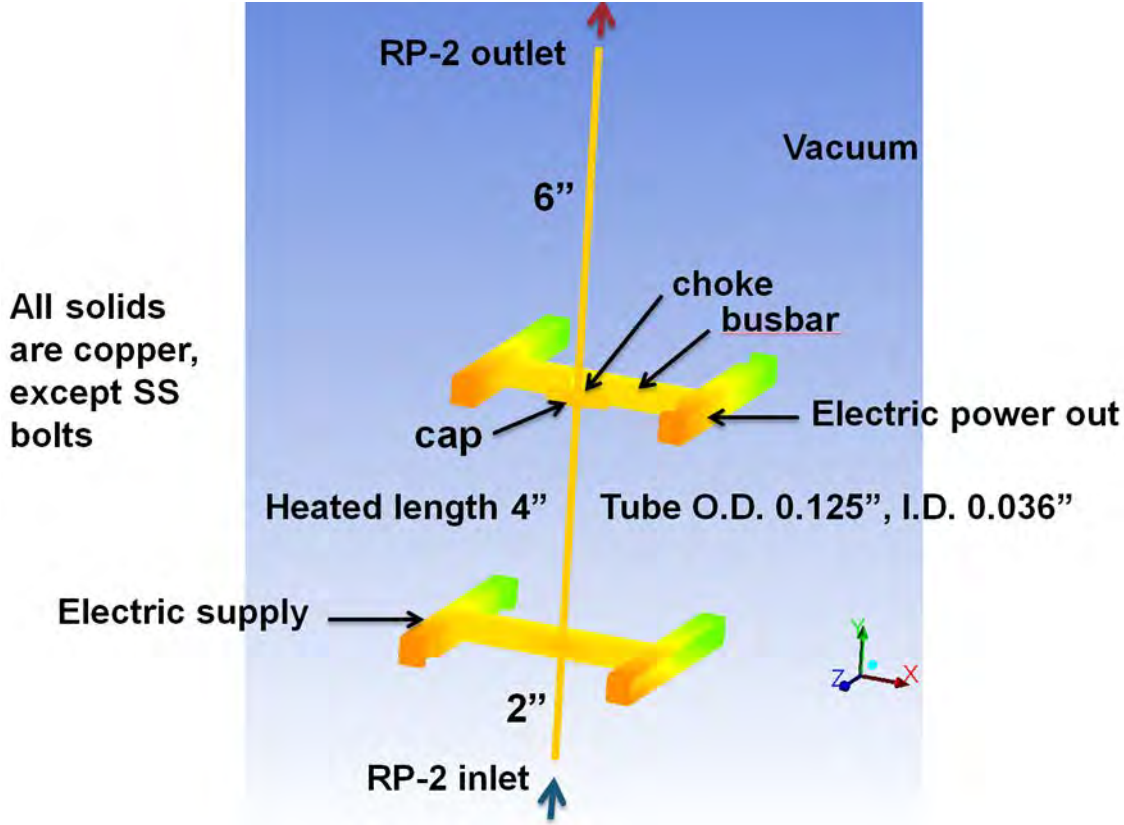


Figure 1. Representation of CRAFTI apparatus (surface colored by z-position).

The conditions of the experimental case to be simulated are shown in Figure 2. They are taken as the measured values of the controlled variables averaged over three test runs to reduce the impact of experimental variability, and averaged over the last 100 seconds of each run to approximate the steady state of the test. A power supply controller is used to control the supplied current so that a desired electric power level delivered to the tube is maintained. The back pressure offered by the fluid in the tube is controlled at a desired level, and the fuel volume flowrate at the inlet is also controlled to a desired level. The fuel inlet temperature is measured by a thermocouple a little upstream of the inlet location shown in the figure. The rounded-up values of the controlled variables for the present test case are shown in Figure 2

Figure 3 shows the applied simulation boundary conditions corresponding to the test case. The back pressure applied at the tube exit 6 in. downstream of the heated section was held at the experimental back pressure, although the locations of these two pressures differ, the experimental one being 6 in. further downstream. The pressure in the tube was not used in the equation of state of the RP-2 in the model, and therefore its absolute value is not significant. At the inlet 2 in. upstream of the heated section, a fully developed turbulent flow profile was applied for the velocity components, the turbulent kinetic energy and the specific dissipation rate. These were obtained for a flow of 0.004035 kg/s, which corresponds to the experimental volume flowrate at the inlet temperature. The inlet temperature of the fuel was also specified to match the experimental value. The electric power was not specified to match the experiment. Instead the electric potential difference applied between the busbars was specified as 2V, as shown in the figure. At all exposed copper surfaces, a thermal boundary condition of radiation to a 300 K environment was applied. At the faces on the busbars which are connected to the power supplies, the experimentally measured temperatures were specified as thermal boundary conditions. This was done because the heat flux from the busbars to the power supply connectors is unknown.

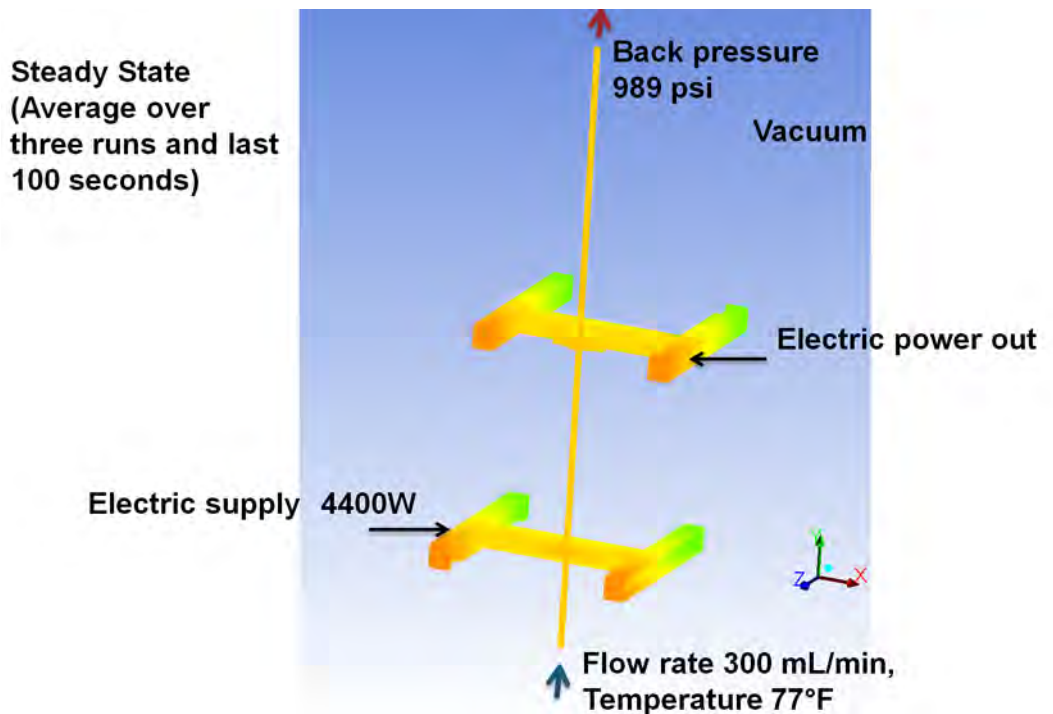


Figure 2. Experimental Case Control Conditions

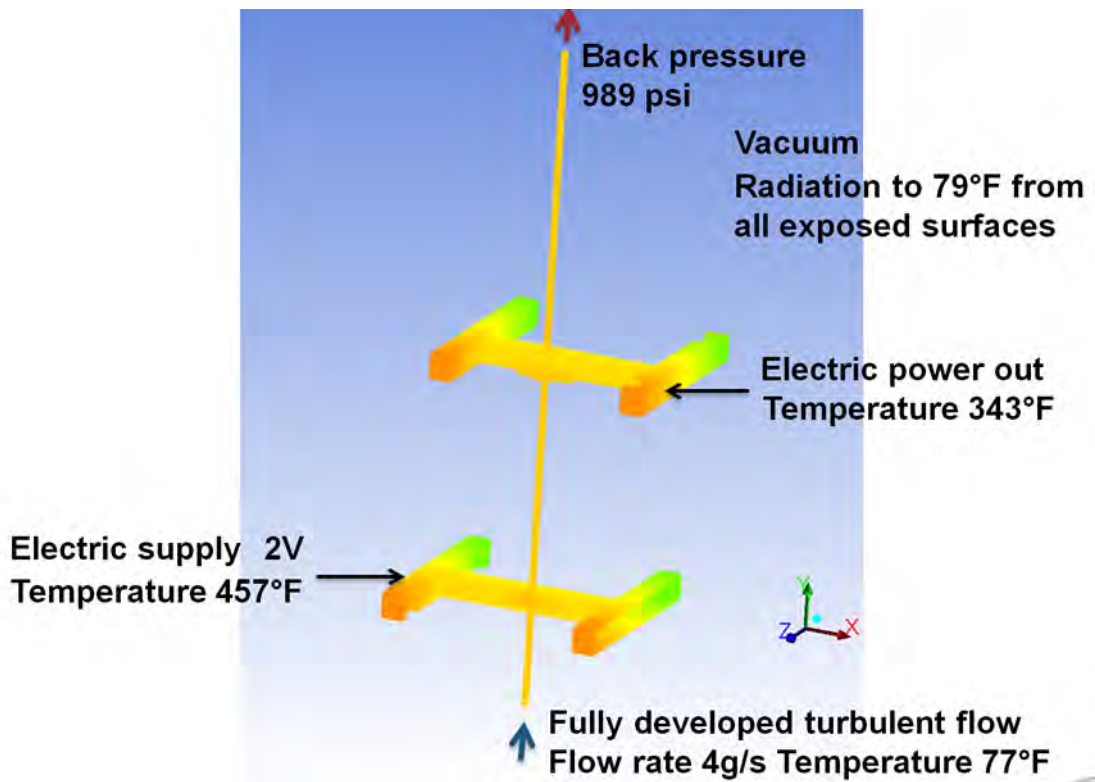


Figure 3. Simulation Case Boundary Conditions.

III. Analytical Model and Numerical Approximation

In the test case, the pressure of RP-2 in the tube is well above its critical pressure of 2.2859 MPa. Because of the very small dependence of density on pressure at such high pressures, the flow is assumed to be incompressible. The density varies significantly with temperature. The mean flow is assumed to be steady over the last 100 seconds of the test. Accordingly, the flow in the tube is taken to be steady, incompressible, variable-density, turbulent flow. The presence of stationary fluid turbulence is treated by Reynolds averaging and using a turbulence model. The conservation equations governing the flow are the standard Reynolds Averaged Navier-Stokes (RANS) equations for conservation of mass, momentum and energy of a fluid flow, and are not repeated here. The RP-2 thermodynamic and transport properties required to complete the flow specification are obtained from REFPROP¹ as functions of temperature, at 989 psi. The dependence of the properties on pressure is very slight at such a high supercritical pressure, and was neglected. The required properties are density, specific heat capacity at constant pressure, molecular dynamic viscosity and molecular thermal conductivity. The strong dependence of these properties on temperature is shown in Figure 4. The variations in fluid viscosity over the expected temperature range of 300 K to 900 K are especially large. These strong dependences lead to strong coupling between fluid flow and energy transport, and the variations of properties cannot be neglected in the analysis without incurring large errors in the predicted temperature field.

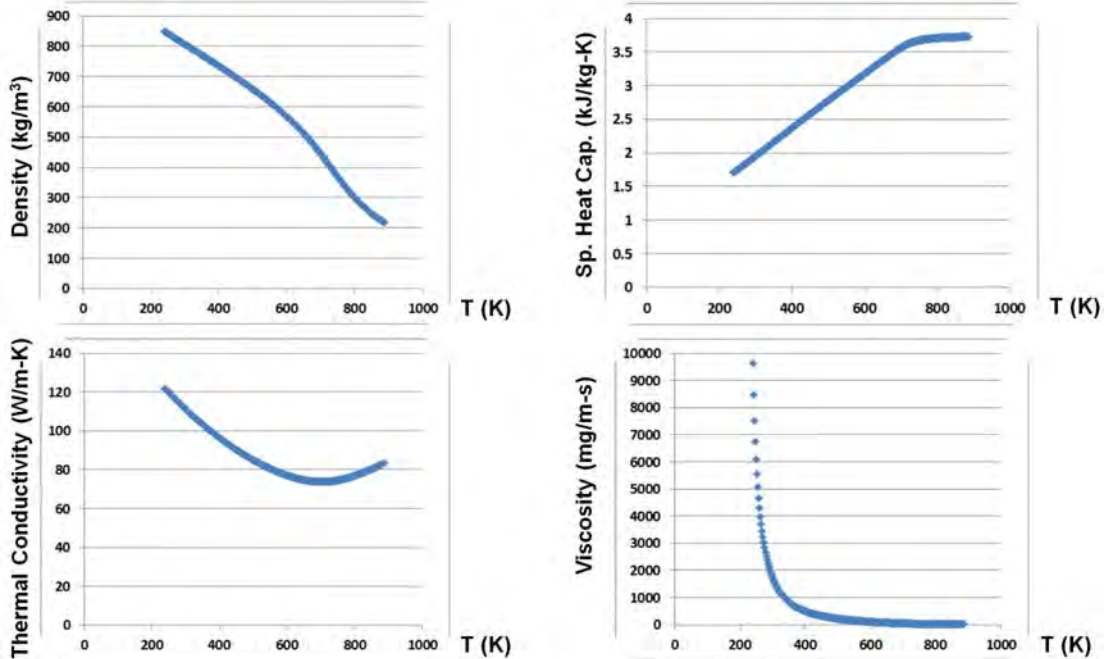


Figure 4. Properties of RP-2 as functions of Temperature.

In the solid domain, the steady flows of both heat and electricity are modeled. The conservation laws of energy and electric current govern the behavior of these phenomena. The thermal and electrical conductivities of stainless steel are much less than those of copper. The presence of the stainless steel bolts was accordingly neglected in the analysis. The heat and the electricity in the solid are strongly coupled. The thermal behavior is strongly influenced by the resistive heating due to the electric current, while the flow of current is influenced by the dependence of the electrical conductivity of copper on the temperature field. The conservation of energy model in the solid is the standard heat conduction equation, with the exception of the appearance of the Joule heating rate density as a heat generation source term in the equation.

The flow of electricity in the metal is modeled with continuum electric current flow field theory as described in many textbooks of electrical engineering or university physics, for example in Ref. 2. The relevant field quantities are the scalar potential V , field intensity vector \vec{e} , current flux density vector \vec{j} , scalar conductivity σ , and scalar Joule heating J . The standard relationships among these quantities are as follows. The relation between force and the work performed by the force is

$$\vec{e} = -\nabla V \quad (1)$$

The conservation law of electric charge for steady currents with no interior charge sources is

$$\nabla \cdot \vec{j} = 0 \quad (2)$$

while the constitutive law for a continuum is

$$\vec{j} = \sigma \vec{e} \quad (3)$$

By eliminating two of the quantities using the above equations, we are left with a governing equation for the potential:

$$\nabla \cdot (\sigma \nabla V) = 0 \quad (4)$$

This involves only a single unknown field, the electric potential. The electrical conductivity is a known function of temperature for any given material medium.

Joule or resistive heating is the conversion of electric power into heat while driving current against electric resistance. The expression for the Joule heating power density is

$$J = \sigma \nabla V \cdot \nabla V \quad (5)$$

This expression is used as a heat generation rate source term in the energy conservation equation in the solid.

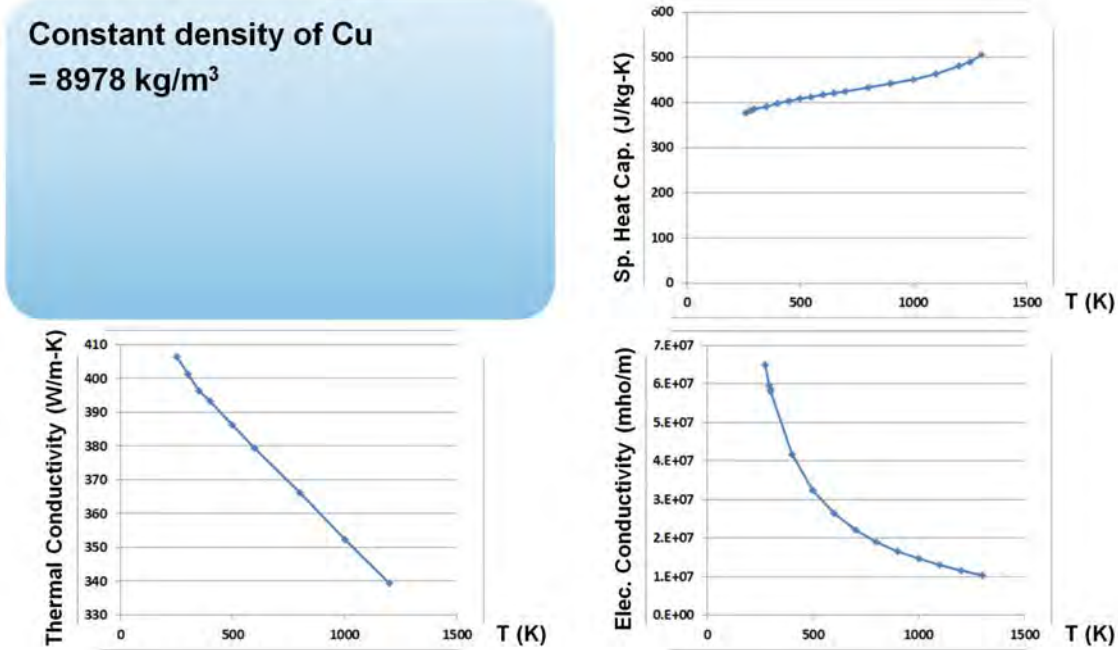


Figure 5. Properties of Copper as Functions of Temperature.

Figure 5 shows the relevant properties of copper that are used in the energy and current conservation equations. The specific heat capacity, thermal conductivity and electrical conductivity values are obtained from Refs. 3, 4 and 5, respectively. The strong dependence of electrical conductivity on temperature plays an important role in the behavior of the Joule heating in the simulation.

The physics in the fluid and solid domain are strongly coupled by heat transfer at the fluid-solid interface, which is the “wet” inner wall of the test article. The coupled fluid-solid heat transfer problem is known as the conjugate heat transfer problem. In solving this problem, the temperature and heat flux at each point of the fluid-solid interface emerge as part of the solution rather than being prescribed as boundary conditions.

The conservation law based model was assembled in ANSYS Fluent 15 simulation software. The option for SST (Shear Stress Transport) $k-\omega$ turbulence model with low Reynolds number corrections was selected. Perfect thermal and electric contact was assumed at all metal-metal interfaces. Analysis presented in the Results and Discussion section shows that the perfect metal-metal contact assumption may not hold in the experiment. It is recommended that the implications of this possibility be investigated in future modeling work. The governing equation for the electric potential field was implemented in Fluent 15 using the User-Defined scalar Transport and

User-Defined Function facilities available in Fluent. Polynomial curve fits to represent the temperature dependence of the fluid and solid thermodynamic and transport properties were entered into Fluent for use in the simulation.

The main heat loss from the tube wall is to the fuel by conjugate heat transfer. Without accounting for the temperature dependence of the fluid properties, the model greatly under-predicts the cooling efficacy of the fuel, which leads to very high wall temperatures. It was found that even after properly accounting for variable fluid properties, when a simulation was performed with a commonly assumed value of 1.5 microns for the copper inner tube wall surface roughness, the cooling efficacy of the fuel was under-predicted, and wall temperatures significantly higher than seen in the experiment were obtained. The interest in the current simulation is focused on the thermal state of the solids. To achieve a fuel cooling efficacy in the simulation similar to that seen in the experiment, the inner wall surface roughness was set to 9 microns.

The simulation was performed using a hybrid unstructured and structured mesh with about 1.75 million cells. The fluid domain and the tube wall were discretized with a structured mesh, while the rest of the solids were discretized with an unstructured mesh. The nondimensional y^+ mesh spacing at the tube inner wall ranged from about 3 in the cold upstream region to about 75 in the heated region. Various views of the mesh can be seen below, in Figures 6 through 9.

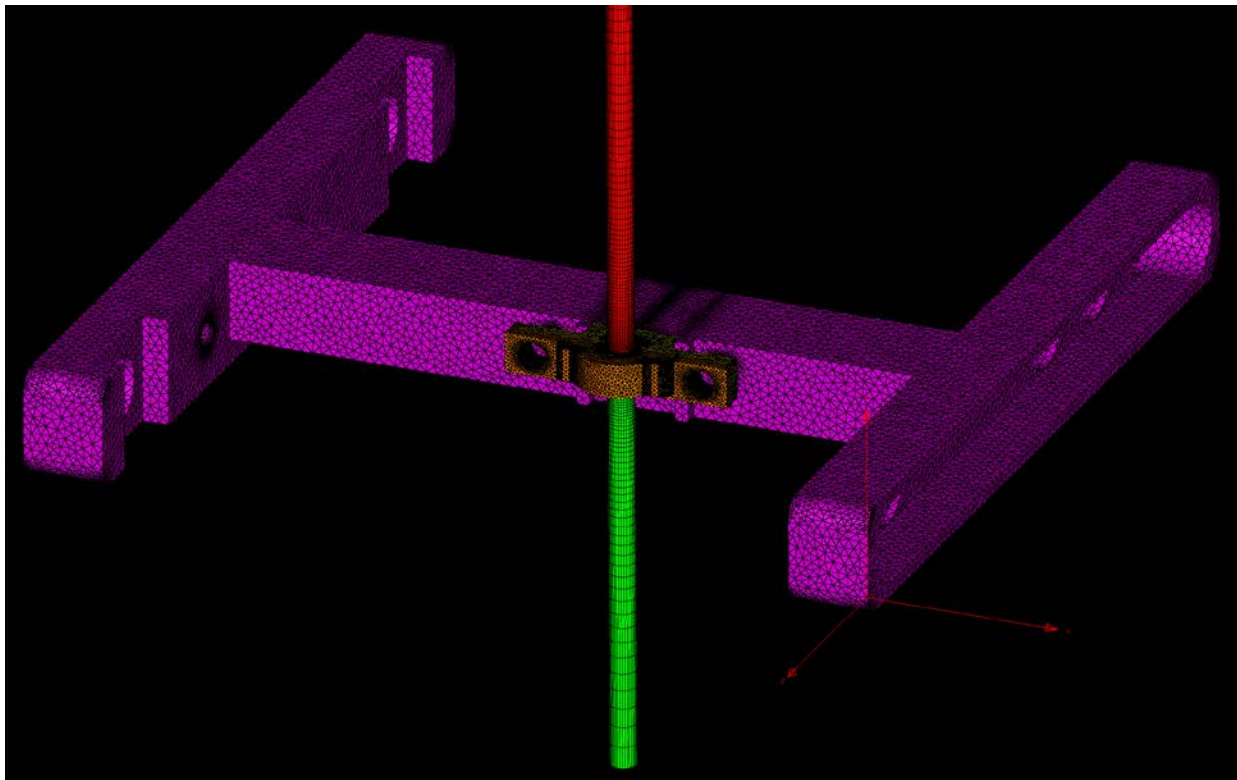


Figure 6. View of Surface of Bottom Half of Mesh.

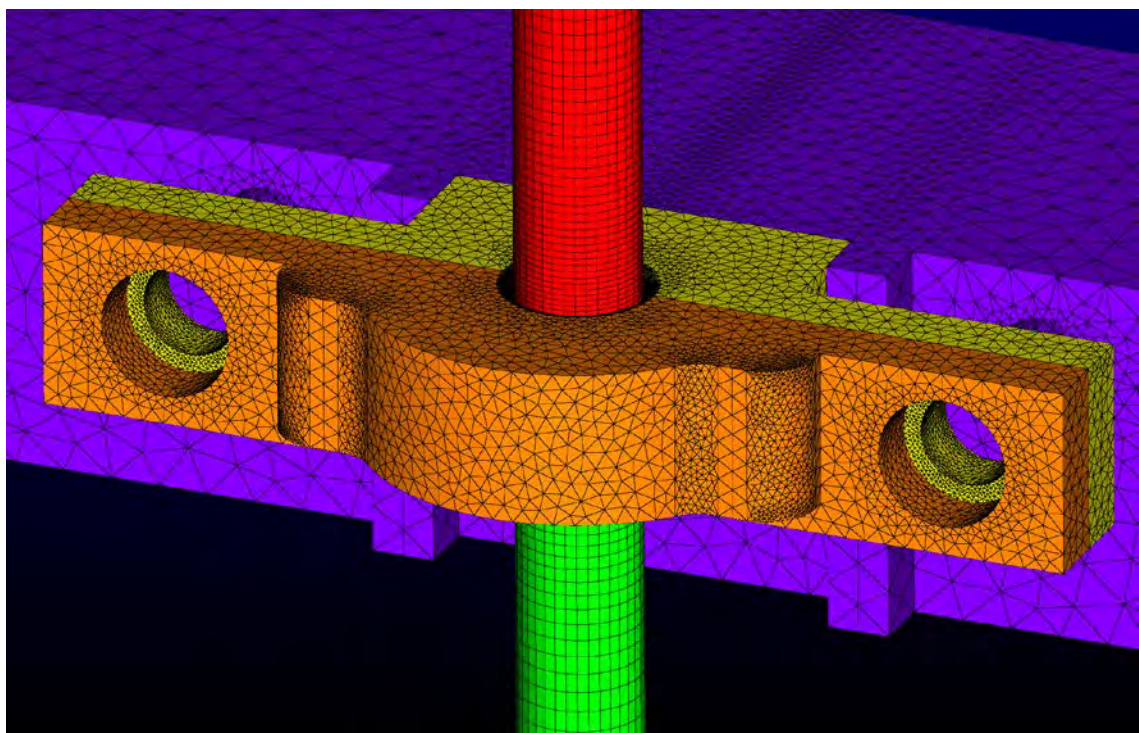


Figure 7. Close-Up View of Inlet Busbar, Inlet Choke, Inlet Cap and Tube.

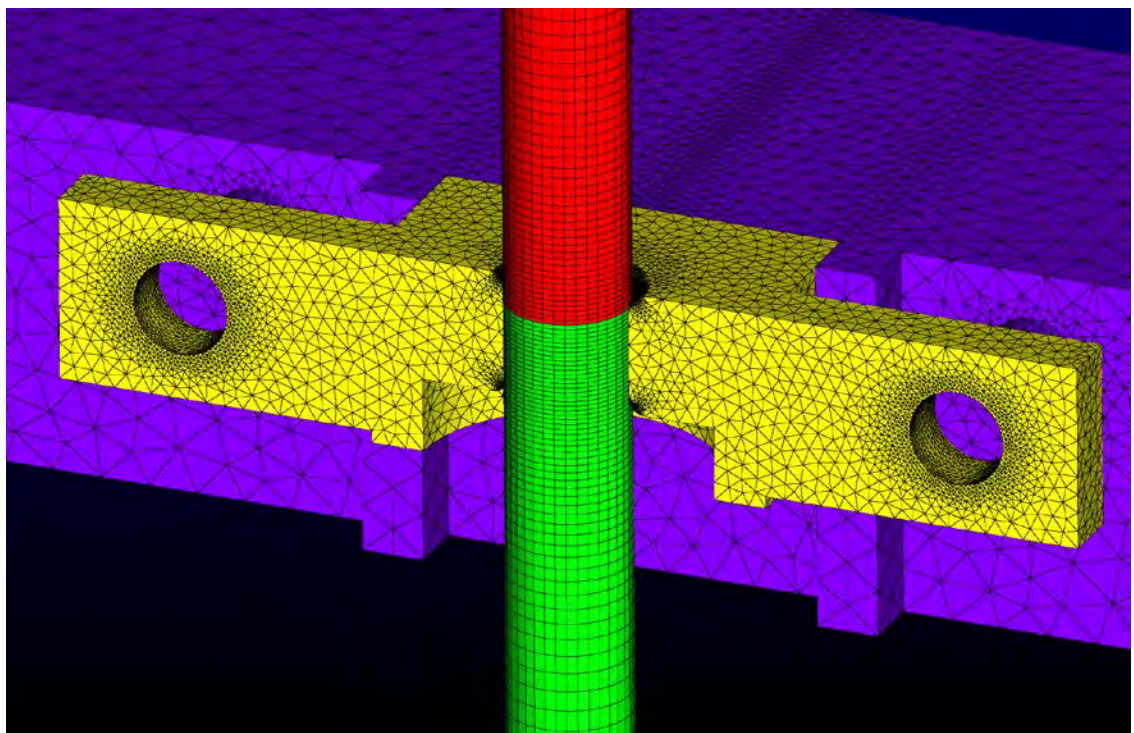


Figure 8. Close-Up View of Inlet Busbar, Inlet Choke and Tube, with Cap Removed.

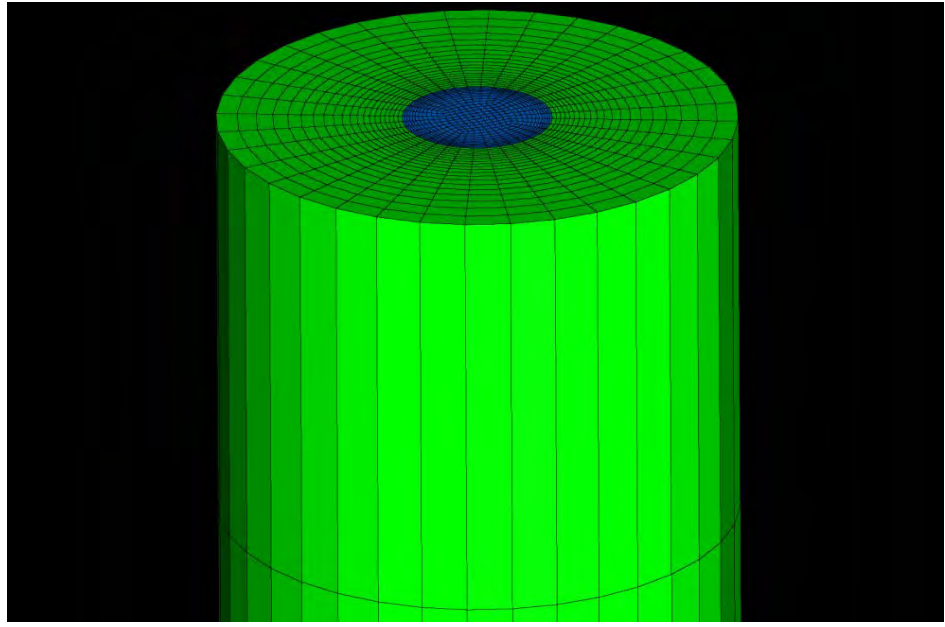


Figure 9. Structured Mesh in Tube Wall (Green) and Fluid (Blue) At Tube Outlet.

IV. Results and Discussion

The results of the simulation are shown below, in Figures 10 through 29. All Figures except for Figure 10 show results from the simulation which used an inner wall surface roughness of 9 microns.

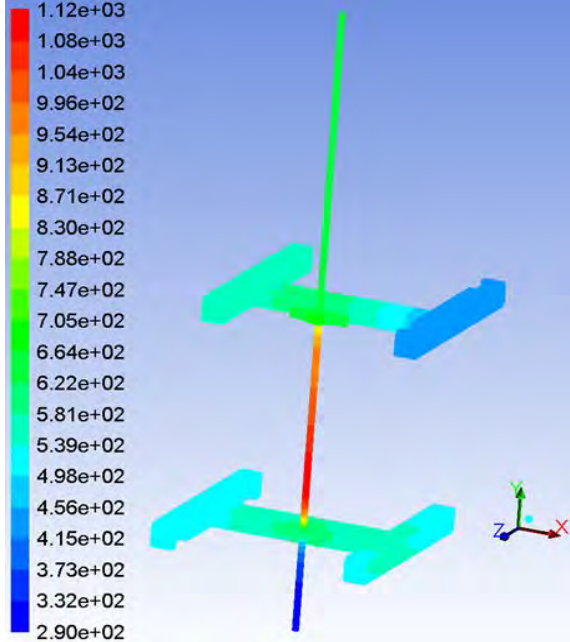


Figure 10. Contours of Surface Temperature (K) for the simulation with tube inner wall surface roughness of 1.5 microns.

In the surface temperature contours of Figure 10 that when a commonly-cited value of 1.5 microns is used for the surface roughness, the tube wall temperatures exceed 1100 K. Examination of the solution showed that while the average temperature difference between tube wall and fuel was higher in this simulation than in the experiment, the rise in bulk temperature of the fuel between inlet and outlet was less in the simulation than in the experiment. This showed that the “cooling efficacy” of the fuel in the simulation as represented by the average surface heat transfer coefficient is underpredicted by the simulation. It was judged that because this simulation inadequately captures the cooling effect of the fuel, it does not yield insight into the thermal state of the busbars, chokes, caps and tube. Therefore it is not presented here in any greater detail. Analyses, not reported here in any detail, were performed of the sensitivity of the heat transfer rate to various aspects of the model. Based on these analyses, the inner wall surface roughness was identified as the only model parameter among

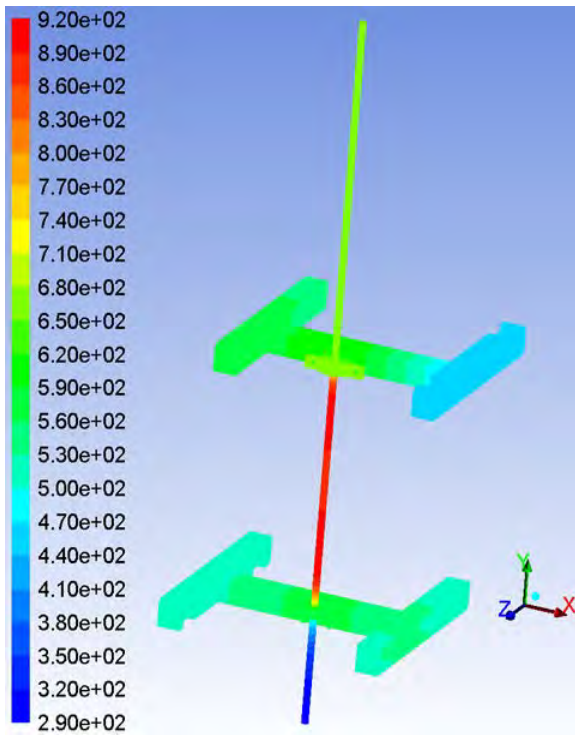


Figure 11. Temperature (K)

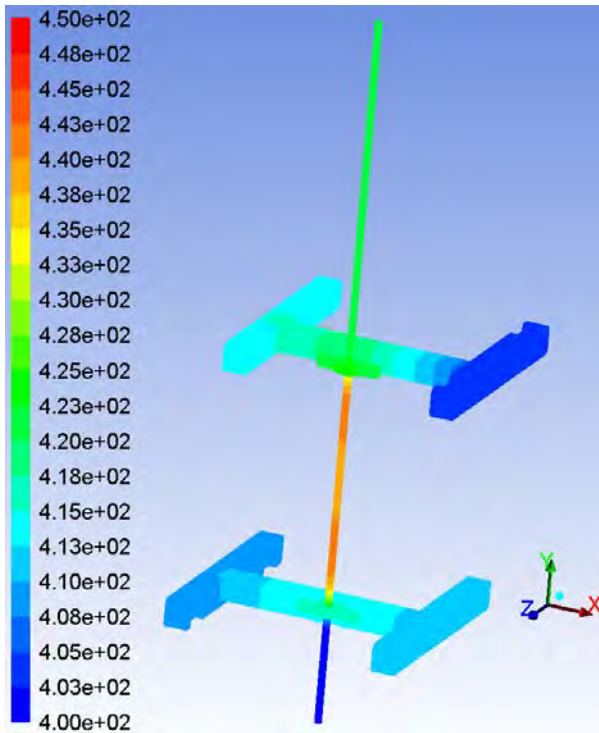


Figure 12. Specific Heat Capacity (J/kg-K).

those investigated that both (a) has a significant effect on the heat transfer to the fuel and (b) about the applicable value of which there is some uncertainty. The uncertainty stems from a lack of knowledge about manufacturing tolerances achieved during the fabrication of long tubes with such a small inner diameter. It was decided to assume a suitable value of the surface roughness, and it was found by trial and error that a not implausible value of 9 microns yields a cooling efficacy in the simulation that roughly matches that seen in the experiment. This value was used for the simulation results presented in all figures other than Figure 10. From the temperature contours in Figure 11, it is seen that there is a large variation in temperature along the tube wall, ranging from about 300 K upstream to about 900 K in the electrically heated portion. The surface temperatures approximately reflect the temperatures that occur in the interior of the solids, though they are slightly lower.

Figures 12 and 13 show appreciable property variations in the copper that reflect the temperature variations seen in Figure 10.

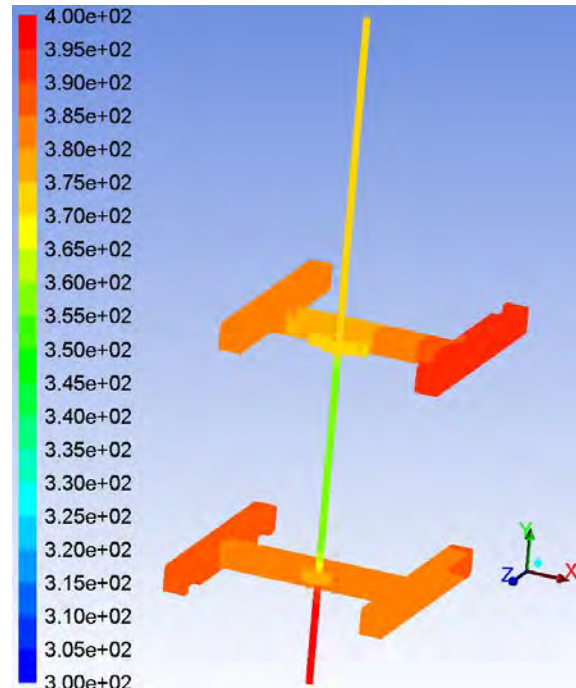


Figure 13. Thermal Conductivity (W/m-K).

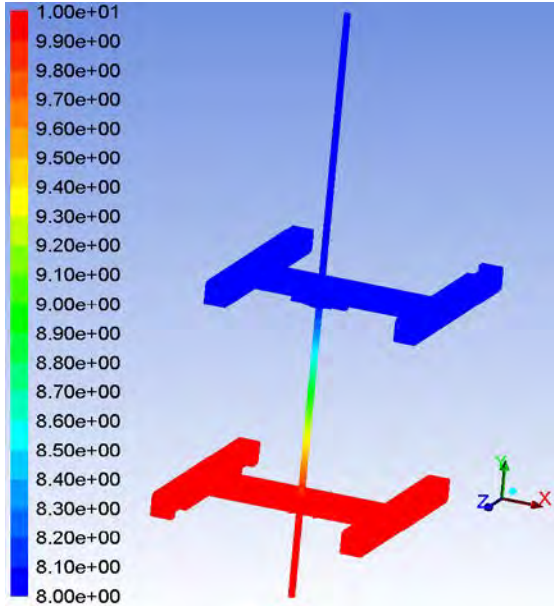


Figure 14. Electric Potential (V).

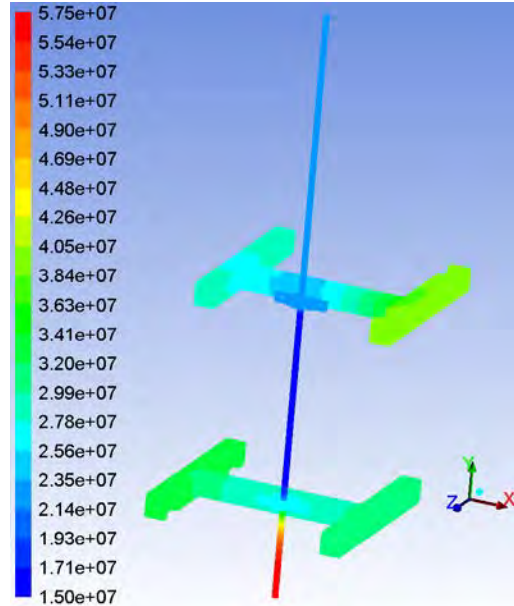


Figure 15. Electrical Conductivity (mho/m).

It is seen from Figure 14 that almost the entire electric potential drop happens along the portion of the tube between the busbars. This is because the tube wall has the smallest cross-sectional area of any part of the current path, and therefore the highest electrical resistance. Furthermore, the heated tube wall is also hotter than the busbars, and therefore has lower electrical conductivity as seen in Figure 15. This increases the fraction of the potential drop that takes place along the tube. The same total current flows through each busbar and through the tube. Therefore, most of electrical power dissipated as heat, which is equal to the product of the current and the potential drop, goes to heat up the tube.

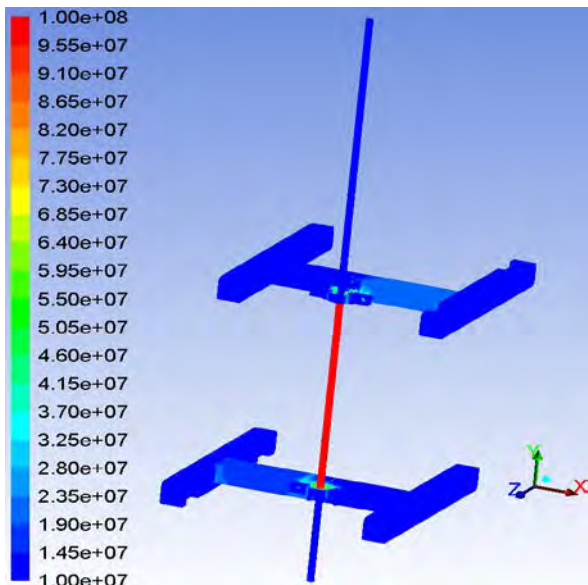


Figure 16. Current Flux Density (A/m^2).

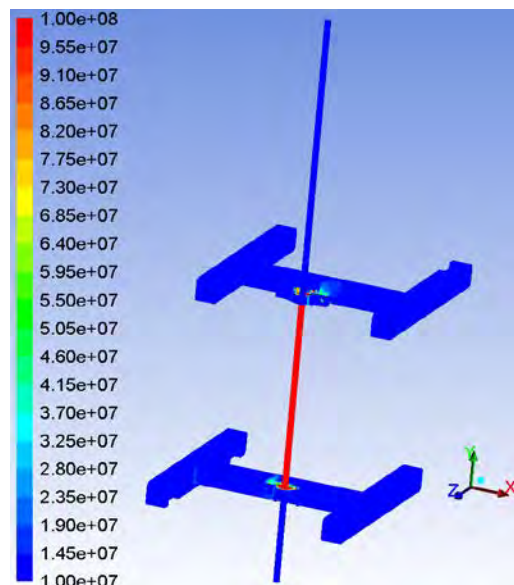


Figure 17. Joule Heating Density (W/m^3).

In Figure 16, the magnitude of the current flux density vector is seen to be highest in the tube wall, but there are appreciably large values in the thermal chokes and their vicinity. This is reflected in the Joule heating heat generation rate density shown in Figure 17, where the localization of Joule heating in the tube and chokes is even more pronounced than for the current flux density, because the former varies as the square of the latter.

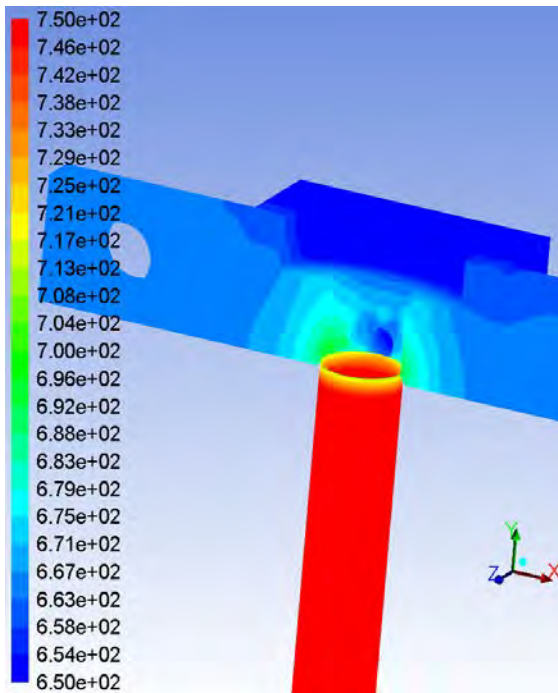


Figure 18. Temperature (K) at Juncture of Tube and Exit Thermal Choke.

The nature of this localization is seen more clearly from Figures 18 through 23. In Figure 18, a close-up view of the junction between the tube and the exit (upper) choke, part of the tube has been removed in order to see the choke surface. The busbar has also been removed from the figure, so that only the choke and tube are seen. In Figure 19 the tube has been removed entirely and in Figure 20, the temperature is shown in a cross-section, which includes the cap and busbar, at the exact y location that the tube starts to make contact with the choke and cap.

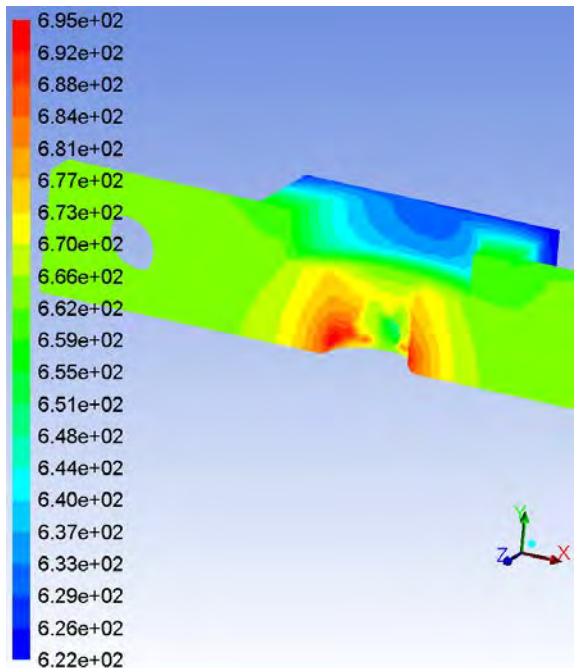


Figure 19. Temperature (K) on Exit Thermal Choke.

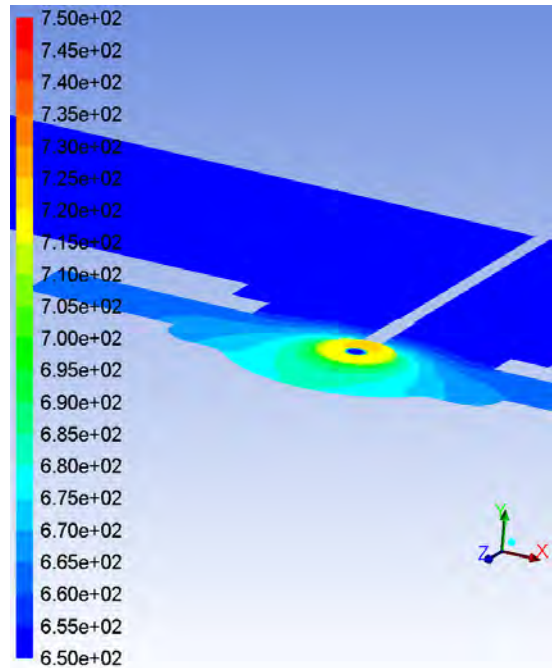


Figure 20. Temperature (K) at Exit Thermal Choke in Section at $y=6.015625\text{in}$.

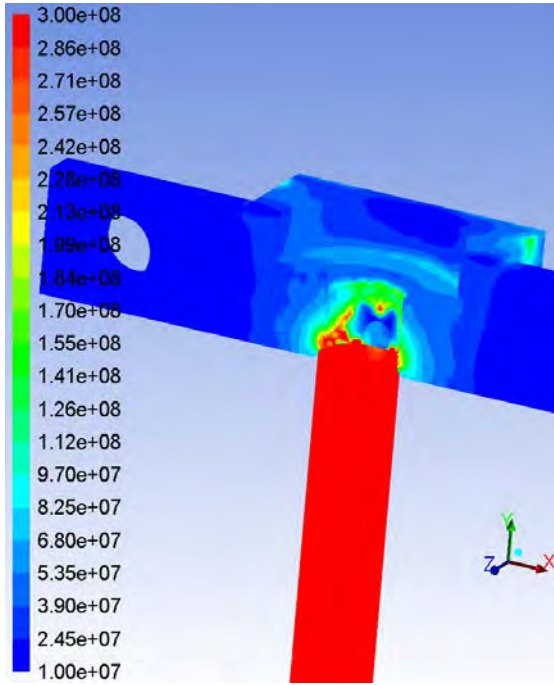


Figure 21. Current Flux Density (A/m^2) at Juncture of Tube and Exit Thermal Choke.

Similar views as for the temperature are shown in Figures 21 through 23 for the current flux density and the Joule heating. From these figures it is evident that the current takes a narrow path from the tube to the choke, and does not equally utilize the entire contact interface between tube and choke to move from one to the other. This is a consequence of the current preferentially traveling along the path of least resistance, in this case the shortest path. As seen from Figure 23, this pattern results in a narrow ring of concentrated Joule heating, leading to localized high temperatures. In the present simulation, the high temperatures are still safely below the melting point 1358 K of copper. However, in the situation that the choke is for any reason in a hotter state than here, this narrowing of the current path may lead to local melting and failure of the choke or tube. Also, the non-uniform temperature distribution in the choke results in non-uniform thermal expansion, localized thermal stresses and possible degradation of good thermal and electrical contact between choke and tube or between choke and busbar. There is a similar phenomenon at the junction of inlet (lower) choke and tube.

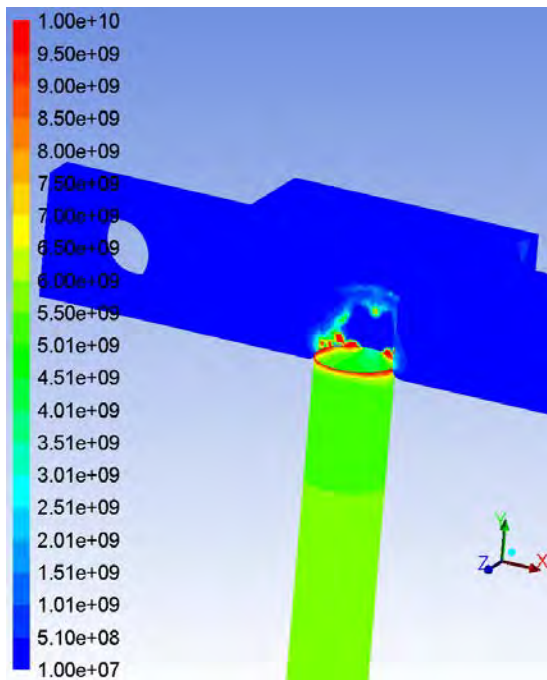


Figure 22. Joule Heating Density (W/m^3) at Juncture of Tube and Exit Thermal Choke.

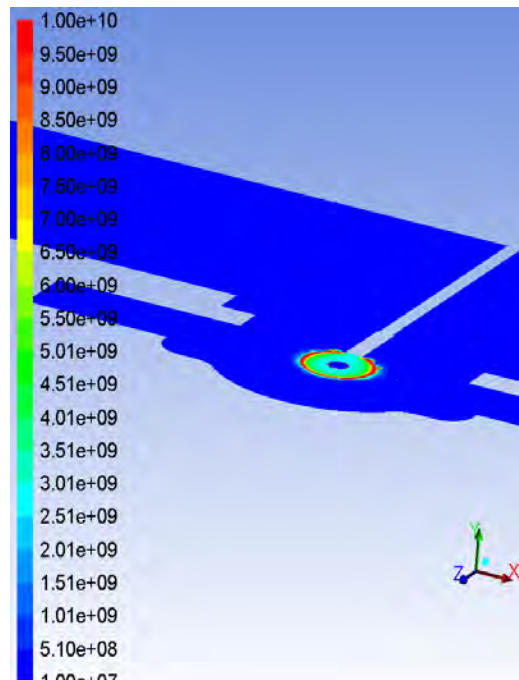


Figure 23. Joule Heating Density (W/m^3) at Exit Thermal Choke in Section at $y=6.015625\text{in}$.

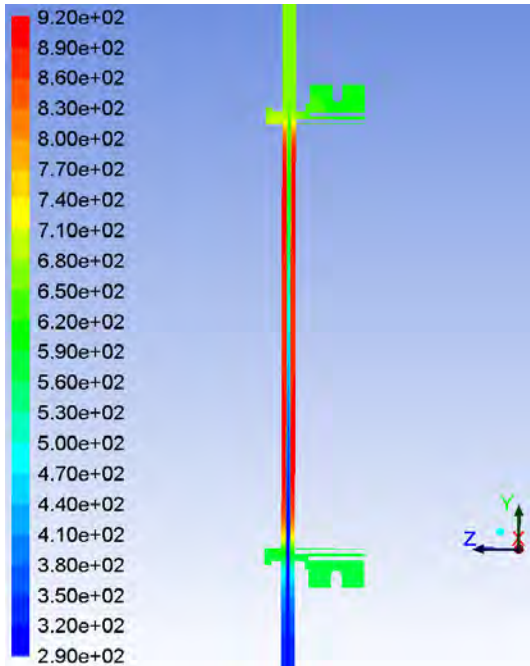


Figure 24. Temperature (K) in Cross-Section at $x=0$.

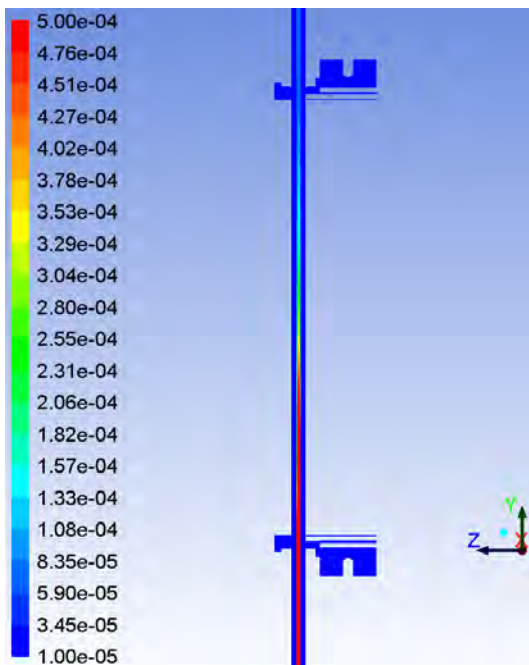


Figure 25. Fluid Viscosity ($\text{kg}/\text{m}\cdot\text{s}$) in Cross-Section at $x=0$.

Turning to the cross-sections of the apparatus at $x=0$ that are seen in Figures 24 through 26, the RP-2 undergoes large changes in the bulk values of temperature and viscosity in the course of its travel through the heated portion of the tube. This affects its performance as a coolant. In Figure 26, the level of turbulent kinetic energy in the core of the flow is seen to drop somewhat in the middle stretch of the heated tube, before picking up again as it nears the exit busbar location.

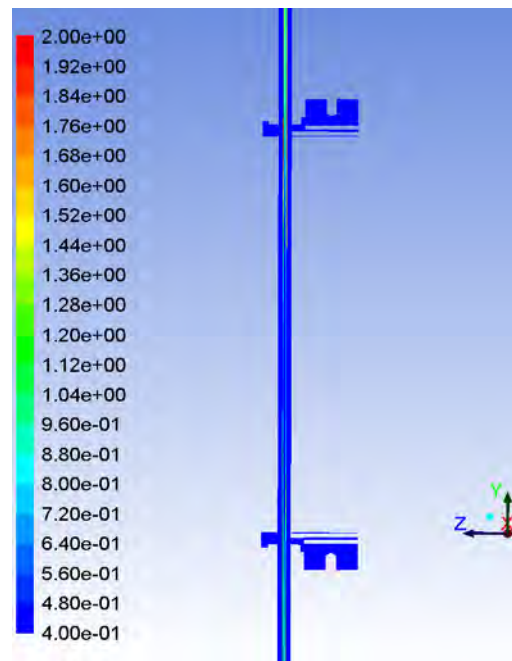


Figure 26. Turbulent Kinetic Energy (m^2/s^2) in Cross-Section at $x=0$.

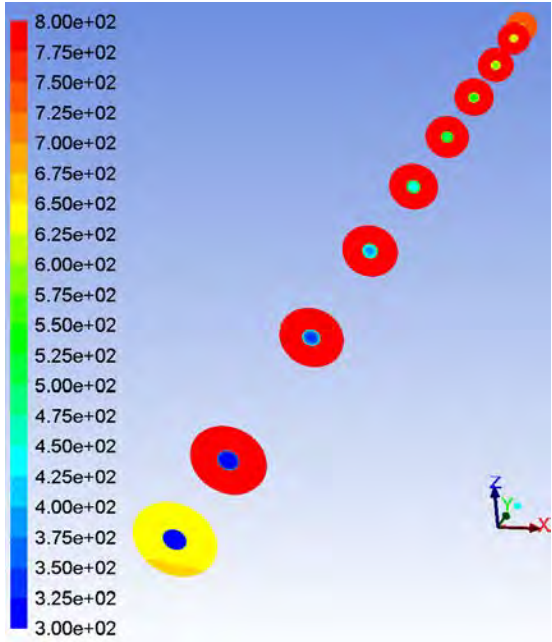


Figure 27. Temperature (K) in Cross-Sections at Thermocouple Locations.

The same rise in fluid bulk temperature is seen in the tube cross-sections taken at the locations of experimental thermocouple measurements and shown in Figure 27. In Figure 28, the magnitude of the current flux density vector is plotted in the same cross-sections. It is seen that because of the lower temperature and higher electrical conductivity near the tube inner wall, as compared with the rest of the tube wall, the current flux density is highest near the inner wall. The current is once again following the path of least resistance. This concentration is seen to be even more pronounced in the Joule heating density contours shown in Figure 29. Thus, because of temperature differences, the Joule heating is unevenly distributed and is strongest at the inner tube wall.

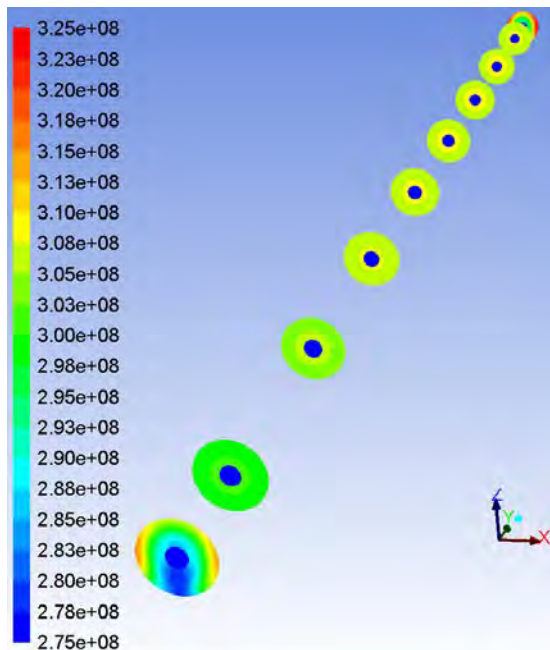


Figure 28. Current Flux Density (A/m^2) in Cross-Sections at Thermocouple Locations.

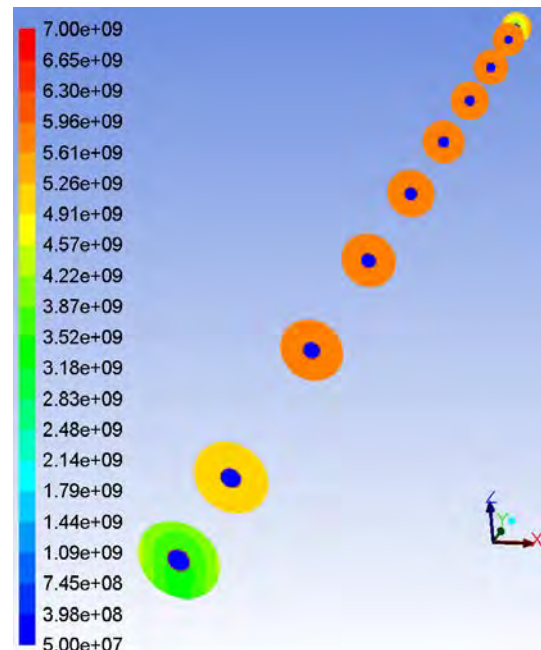


Figure 29. Joule Heating Density (W/m^3) in Cross-Sections at Thermocouple Locations.

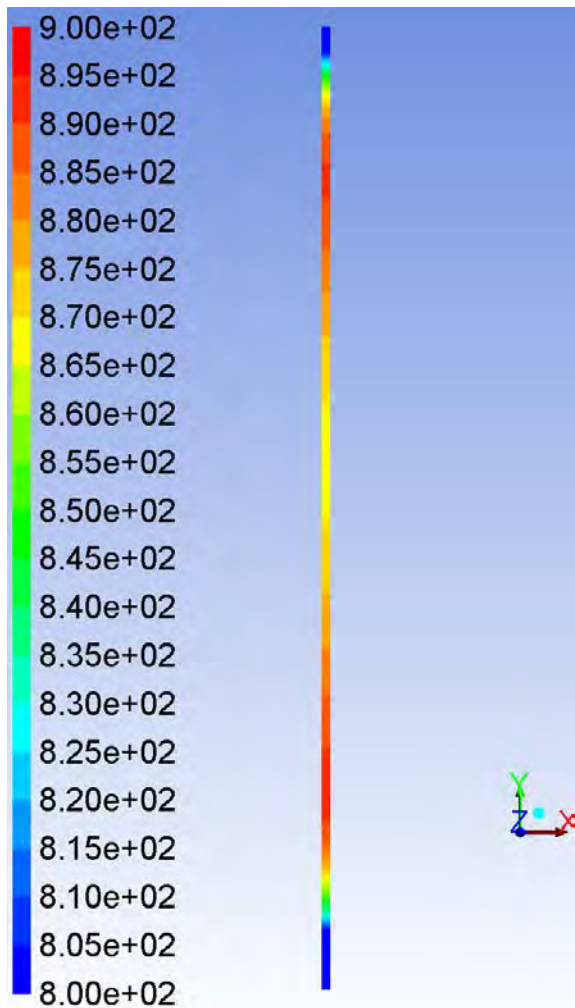


Figure 30. Temperature (K) at the Tube Wall Inner Surface in between Thermal Chokes.

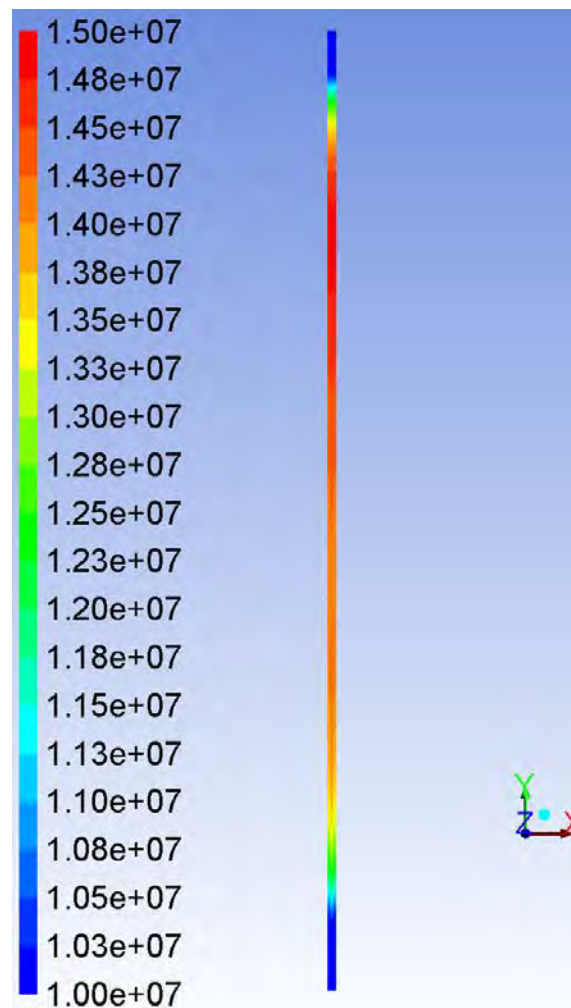


Figure 31. Heat Flux (W/m^2) at the Tube Wall Inner Surface in between Thermal Chokes.

Next, we examine thermal conditions at the tube wall inner surface in the portion of the tube between the two busbars. This is the interface between fluid and solid where the principal heat transfer occurs from tube wall to fuel. Figure 30 shows contours of the temperature on this cylindrical surface. There is a variation of over 100 K over the four inch length, with a dip in the temperature in the central portion. The surface-normal heat flux contours are shown in Figure 31. End effects of significant axial extent are seen, in which the heat flux dips as much as a third below its peak value. This is in contrast to the ideal heat flux distribution of uniform heat flux over the same length.

We turn next to a comparison between the simulation data and the experimental data. Table 1 shows both values of the variables that are controlled in the experiment, for both experiment and simulation. The volume flowrate of RP-2 as well as its inlet temperature match between experiment and simulation, of course, because we have set up the simulation to do so. The two back pressures also match, though they are enforced at different locations. The back pressure is set in the experiment much further downstream than in the simulation. As previously noted, the absolute value of the back pressure specified in the simulation has no significance, because the pressure dependence of the equation of state of RP-2 has been neglected. The electrical power predicted by the simulation is a little less than that set in the experiment. In the simulation, the power delivered was not adjusted by adjusting the voltage. Rather, the voltage was adjusted so that the average predicted tube wall temperatures approximately matched those measured in the experiment. The net current through the tube wall was calculated in post-processing, and the predicted electrical power was calculated as the product of the voltage and the current. If the potential difference

(voltage) set in the simulation is raised above the value of 2 in order to match the power level set in the experiment, a larger current would flow in the apparatus, but the tube wall temperatures would be significantly higher than seen in the actual experiment. This is in spite of having adjusted the surface roughness to 9 microns in order to get approximately the right fuel cooling efficacy. The matching of cooling efficacy would mean that the inner wall surface heat transfer coefficient would match between simulation and experiment.

| Controls | Exit Pressure | Vol. Flowrate | Inlet Temp. | Elec. Power |
|------------|---------------|--------------------|-------------|-------------|
| | MPa | cm ³ /s | K | W |
| Experiment | 6.821688 | 4.9975 | 298.34 | 4415.33 |
| Simulation | 6.821688 | 4.9975 | 298.34 | 4344.44 |

Table 1. Experiment Control Variables: Measured Values in Experiment and Simulation.

In order to provide useful information, the CRAFTI experiment was designed to measure several output variables in addition to the case conditions listed in Table 1. The locations of some of these output measurements are approximately indicated in Figure 32, and the output variables selected for examination are listed in Table 2. The output variables include the voltage drop from one thermal choke to the other, the current passing through the tube, the bulk exit temperature of the fuel, the temperatures at the base of the busbars (shown as BB in the figure), the temperatures of each choke at the junction of the choke with the busbar (not shown in figure), the temperature of an instrumentation collar (not shown in figure) for the tube that was not included in the simulation, and the temperature on the tube outer wall at 10 thermocouple locations numbered TC0 through TC9. TC0 and TC1 are located practically where the tube makes contact with the chokes, i.e. at $y = 2$ in and $y = 6$ in, TC1 is 0.25 in from TC0, TC8 is 0.25 in from TC9, and TC1 through TC8 are spaced 0.5 in apart.

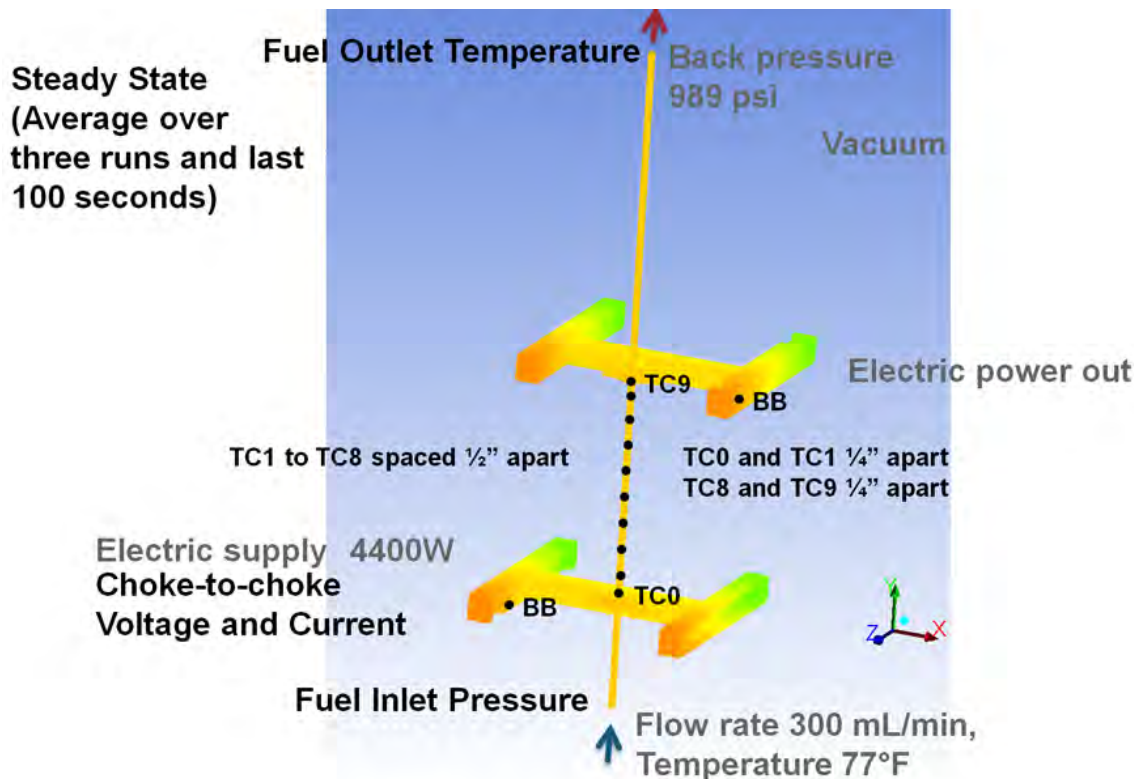


Figure 32. Experimental Output Quantities (Control Inputs are grayed out).

Table 2 lists the experimentally measured values of the output quantities and those predicted by simulation for comparison. The temperatures at the base of the inlet and exit busbars are a match between experiment and simulation. As previously discussed, this is no accident, but is due to the experimental values being used as thermal boundary conditions in the simulation, to compensate for lack of information about heat transfer from the busbars to the environment.

| Output | Volts | Amps | Inlet p MPa | Exit T | Inlet busbar | Exit busbar | Inlet choke | Exit choke | Instr. collar | |
|--------|--------|--------|-------------|--------|--------------|-------------|-------------|------------|---------------|-------|
| Expt. | 2.1426 | 2060.7 | N/A | 661.13 | 509.29 | 445.64 | 881.56 | 929.05 | 508.24 | |
| Smln. | 2 | 2172.2 | 7.2341 | 659.08 | 509.29 | 445.64 | 576.84 | 639.68 | N/A | |
| TC# | 0 | 1 | 2 | 3 | 4 | 5 | 6 | 7 | 8 | 9 |
| Expt. | 742.3 | 897.6 | 909.5 | 890.6 | 862.5 | 883.3 | 878.5 | 909.6 | 886.2 | 777.9 |
| Smln. | 651.0 | 820.3 | 905.9 | 899.3 | 888.2 | 884.0 | 891.5 | 905.1 | 875.4 | 747.0 |

All temperatures in K

Table 2. Experiment Output Variables: Measured Values in Experiment and Simulation.

The temperatures from Table 2 at the thermocouple locations on the heated portion of the tube, both experimentally measured and predicted by simulation, are also plotted for comparison with each other in Figure 33.

From Table 2, the temperatures at the majority of the thermocouple locations on the tube surface, namely TC2 through TC8 are fairly well matched between the experimental and the simulation values. This is also seen in Figure 33. Thus, the thermal state of the tube wall is fairly well matched between experiment and simulation. The simulation also matches the experiment closely with regard to the bulk exit temperature of the fluid. Since the fluid has the same inlet temperature in both experiment and simulation, this means that the heat rejection rate from the tube wall to the fluid is also a close match. In fact, knowing the state of the fuel at inlet and outlet, the inlet and outlet enthalpies can be found from REFPROP. Together with the known flow rate of the fuel, the difference of enthalpies shows that energy is being added to the fuel at the rate of about 3936 W. Taken together with the tube wall being at similar temperatures in both experiment and simulation, we can see that the “cooling efficacy” of the fuel is similar between experiment and simulation. Given the same mass flow rate and tube cross-section between the two, this implies that the surface heat transfer coefficients roughly match.

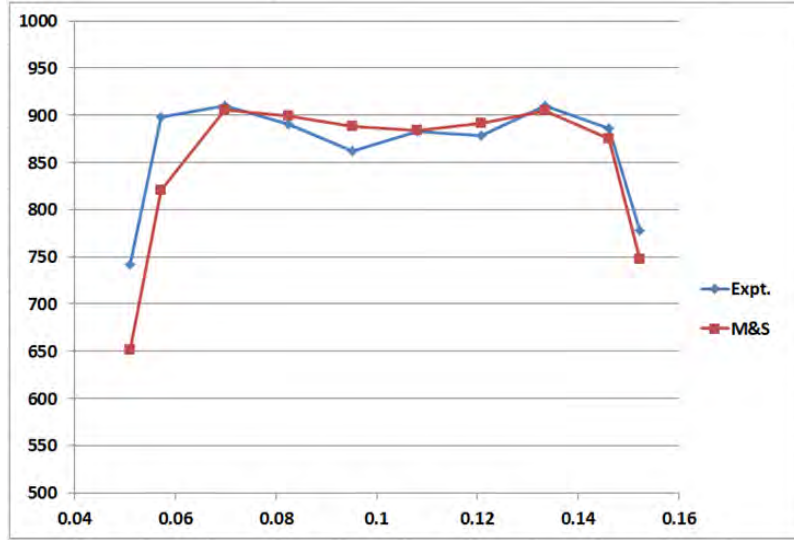


Figure 33. Tube Surface Temperatures – Experimental and Predicted Values.

In the case of the experiment, the tube wall temperatures at either end of the heated length are considerably higher than in the case of the simulation, as seen in Table 2, from the values at TC0, TC1 and TC9. The difference between the two cases is even more extreme when examining the measured and predicted temperatures of the two thermal chokes. These differences suggest that there is an un-modeled thermal resistance between choke and busbar. The resulting high temperatures in the chokes lead to lower electrical conductivity and higher Joule heating in the chokes, which may account for the higher power draw from the supply in the experiment as compared with the simulation. The likely form of this un-modeled thermal resistance is a contact resistance between choke and busbar due to imperfect thermal contact between the two. In experiments where the fuel is being subjected to greater thermal stress with higher tube inner wall temperatures and heat fluxes, a failure mode may manifest due to melting of one of the chokes. The imperfect contact may also manifest as an electrical contact resistance, leading to a greater fraction of the current flowing through the stainless steel bolts instead. This scenario leads to the possibility of a failure mode involving melting of the bolts or a sufficient decrease in tensile yield strength that leads to plastic fracture.

The inlet pressure was predicted by the simulation to be higher than the exit pressure by about 0.4124 MPa. The inlet pressure measured in the experiment, although having a value very close to the 7.234 MPa predicted in the simulation, is not listed in Table 2 because it is in fact measured at a location considerably upstream of the inlet location in the simulation. This implies that the pressure drop occurring over the simulated length of the test article is far less in the experiment than it is in the simulation. This in turn implies that the surface roughness and resulting wall friction in the simulation are significantly higher than in reality. It therefore implies that some other physics, missing from the model, is the reason why the cooling efficacy of the fuel in the experiment is higher than that of the model when the surface roughness is not set artificially high. Possible reasons include uncertainties in surface roughness, fuel properties and turbulence model response to sharp changes in fuel properties.

The measured temperature of the instrument collar in the experiment suggests that the radiation boundary condition for the external tube surface should be set to radiate to an environment of 508.24K rather than to 300K. The condition as used causes the tube wall temperature to drop by about 30K as compared to an adiabatic boundary condition.

V. Summary and Conclusions

Conjugate heat transfer and electric current flow with the rocket kerosene RP-2 flowing in an electrically heated tube was simulated. The model and boundary conditions were selected so as to simulate an experimental case reported in the fuel thermal stability literature. The model included steady, incompressible, variable-density turbulent flow inside the tube, thermally coupled with steady heat conduction and electric current flow in the solid copper apparatus. Accurate temperature dependence of fluid and solid thermodynamic and transport properties was included in the model. All physics are strongly coupled both in the model and the experiment.

The comparison of simulation with experiment led to the conclusion that some unknown physics is missing from or poorly represented in the model, that would enable the simulation to match the experimentally observed cooling efficacy of the fuel. The tube inner wall surface roughness was set to 9 microns in order to match the cooling efficacy of the fuel observed in the experiment. With this setting, the simulation predicted an RP-2 temperature rise in agreement with experiment, and a tube wall thermal state largely in agreement with experiment.

The simulation identified regions of temperature, current flux density and Joule heating concentration. The identified regions are at the junction of the tube with each thermal choke. These concentrations may lead to tube or choke failure in experiments involving higher heat fluxes.

The predicted tube wall temperatures at each end of the heated portion of the test article were significantly less than the experimentally observed values. The predicted temperatures of the thermal chokes were considerably less than the experimentally observed values. The conclusion drawn was that an un-modeled thermal resistance or resistive heating source is present in the experiment. The further conclusion was drawn that this unknown resistance or heating represented a failure risk of the choke in the case of experiments with higher heat fluxes.

VI. Future Work

Based on the findings of this study, the following directions of investigation will be considered in attempts to improve the model's predictive power.

- A simulation of the same experiment will be performed using a mesh with a wall y^+ spacing less than unity, in order to resolve boundary layer heat transfer by a solve-to-wall approach rather than with the use of wall functions as in the current study.
- More accurate fluid properties will be sought, and the dependence of properties on pressure will be taken into account.
- A realistic value of wall surface roughness for the tube inner wall will be used in the turbulence model.
- A cold flow simulation will be performed, and the pressure drop predicted be compared with reliable experimental data.
- The stainless steel bolts binding busbar, choke and cap will be included in the analysis.
- The influence of imperfect thermal and electrical contact between choke and busbar will be studied.
- The fluid mechanics literature will be searched for studies on the response of turbulence and turbulent heat transfer to sharp changes in fluid properties.

The longer-term goal of the modeling and simulation activity is to build the capability to predict thermal stability of fuel flowing in regenerative cooling channels. This will include the chemistry of the formation of insolubles and the fouling of the coolant channels by wall deposits.

References

¹Lemmon, E.W., Huber, M.L., and McLinden, M.O., "NIST Standard Reference Database 23, NIST Reference Fluid Thermodynamic and Transport Properties—REFPROP, version 9.0. Standard Reference Data Program", National Institute of Standards and Technology, Gathersburg, MD, 2010.

²Young, H.D, Freedman, R.A. and Ford, A.L., *University Physics with Modern Physics*, 13th ed., Addison-Wesley, Boston, MA, 2011.

³White, G.K., and Collocott, S.J., "Heat Capacity of Reference Materials: Cu and W", URL:
<http://www.nist.gov/data/PDFfiles/jpcrd263.pdf> [cited 18 June 2015].

⁴efunda, "Thermal Conductivity of Copper", URL:
http://www.efunda.com/materials/elements/TC_Table.cfm?Element_ID=Cu [cited 18 June 2015].

⁵Matula, R.A., "Electrical Resistivity of Copper, Gold, Palladium and Silver", URL:
<http://www.nist.gov/data/PDFfiles/jpcrd155.pdf> [cited 18 June 2015].



Simulation of Rocket-Grade Kerosene Flowing in an Electrically Heated Apparatus

*Propulsion and Energy Forum
27-29 July 2015, Orlando, Florida*

Ananda Himansu, Matthew C. Billingsley
Air Force Research Laboratory

Nicholas Keim, Ben Hill-Lam, Claire Wilhelm
Center for Aerospace-Defense
Research and Engineering

Integrity ★ Service ★ Excellence



Research Context



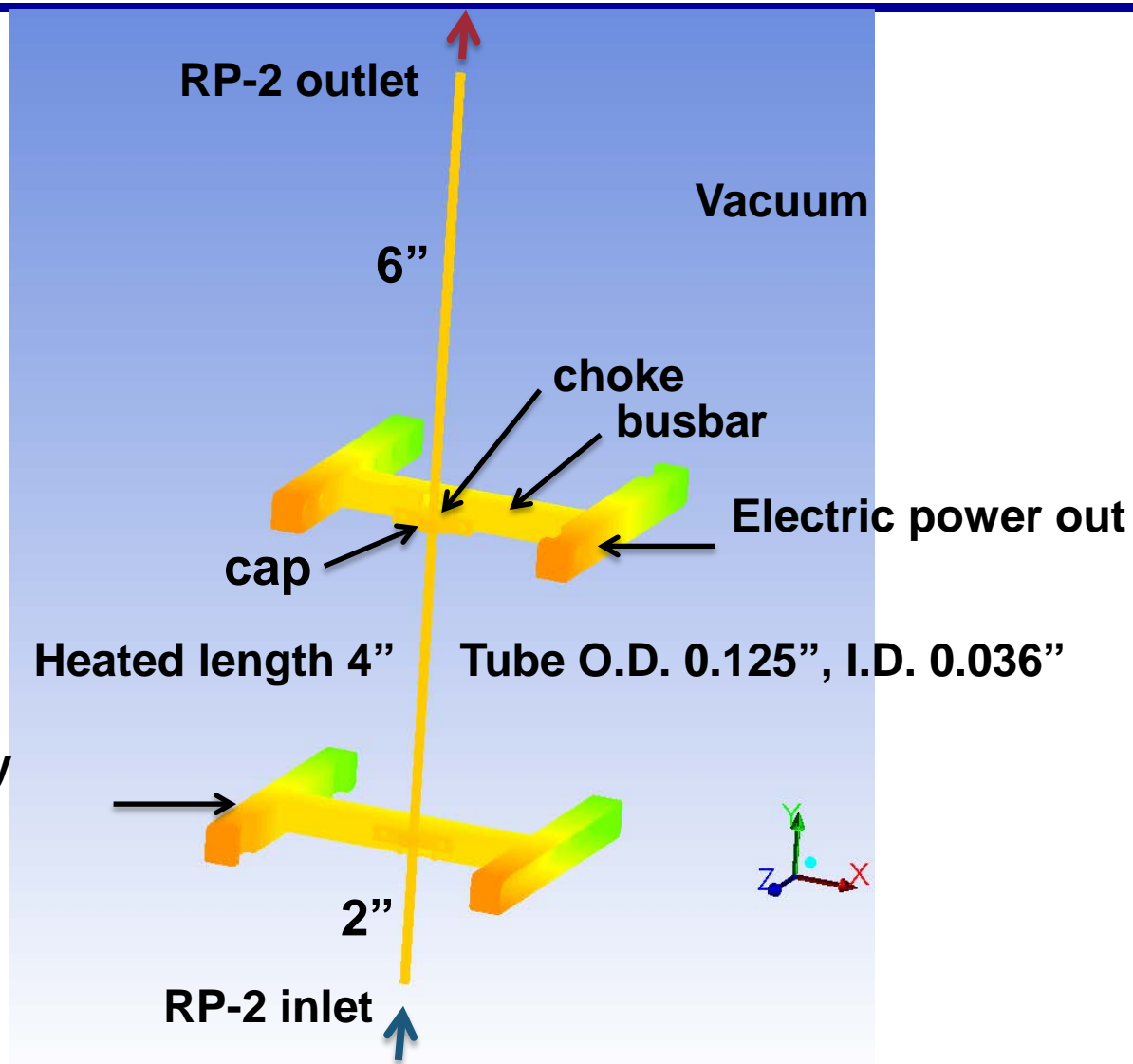
- In-Wall Regenerative Fuel Cooling is a key technology in Liquid Rocket Engines and Hypersonic Aircraft
- The Air Force and NASA are keen to advance thermal management technology involving hydrocarbon fuels
- Advances in cooling efficiency are limited by the thermal stability of hydrocarbon fuels and cooling channel fouling
- The Compact Rapid Assessment of Fuel Thermal Integrity (CRAFTI) rig at CPIAC is aimed at advanced fuels testing
- The current M&S effort is aimed at fuel thermal stability model validation and apparatus design improvement
- Simulation of the experimental case that is reported in
 - Keim, N., et al, “Recent Liquid Hydrocarbon Fuel Thermal Stability Results from the CRAFTI Experiment”, JANNAF, June 2015



CRAFTI Rig Principle

All solids
are copper,
except SS
bolts

Electric supply





Test Conditions

Steady State
(Average over
three runs and last
100 seconds)

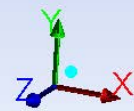
Electric supply 4400W

**Back pressure
989 psi**

Vacuum

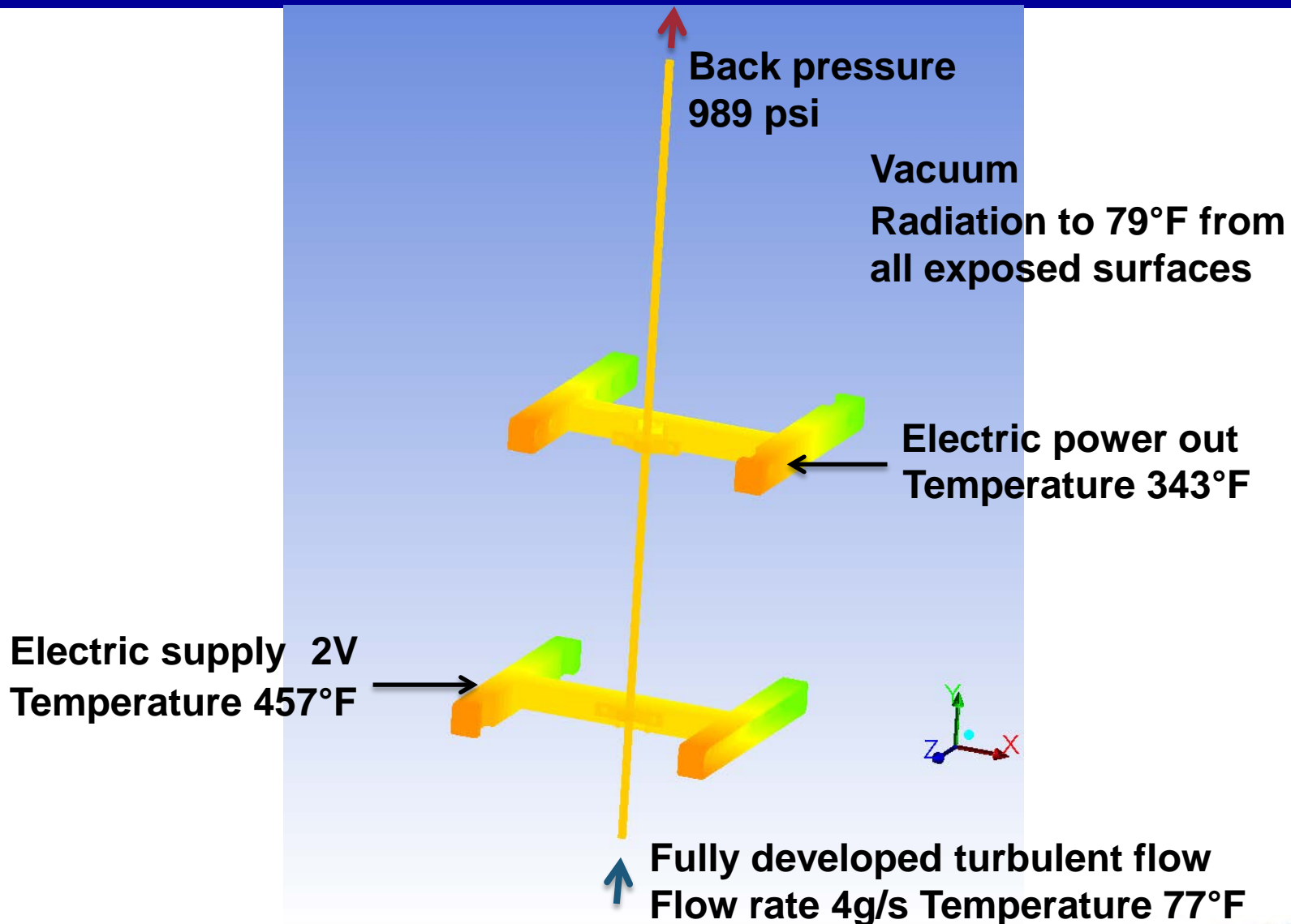
Electric power out

**Flow rate 300 mL/min,
Temperature 77°F**





Simulation Boundary Conditions





Model



- **Fluid**
 - Steady, incompressible, variable-density, turbulent flow at supercritical pressure
 - Conservation of mass, momentum and energy
 - Temperature-dependent fluid properties (slight pressure-dependence is neglected) – strongly couples flow and energy
 - Density, Specific Heat Capacity, Viscosity, Thermal Conductivity
- **Solid**
 - Steady heat conduction and electricity flow
 - Conservation of energy and electric current
 - Heat and electricity are strongly coupled by Joule Heating and temperature-dependence of electrical conductivity
- **Fluid and Solid physics are strongly coupled by heat transfer at fluid-solid interface (conjugate heat transfer)**



Model – Electric Field



- Field quantities are the potential V , field intensity \vec{e} , current flux density \vec{j} , conductivity σ , Joule heating J
- $\vec{e} = -\nabla V$ (relation between force and work)
- $\nabla \cdot \vec{j} = 0$ (conservation law of electric charge for steady currents with no interior charge sources)
- $\vec{j} = \sigma \vec{e}$ (constitutive law for continuum)
- $\nabla \cdot (\sigma \nabla V) = 0$ (governing equation for V)
- Joule or ohmic heating is the conversion of electric power into heat while driving current against electric resistance
- $J = \sigma \nabla V \cdot \nabla V$ (Joule heating source in energy equation)



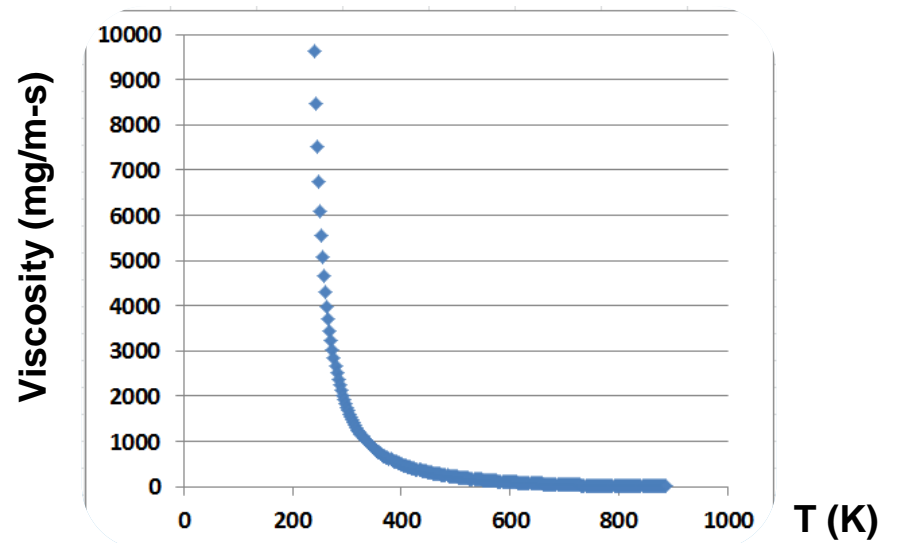
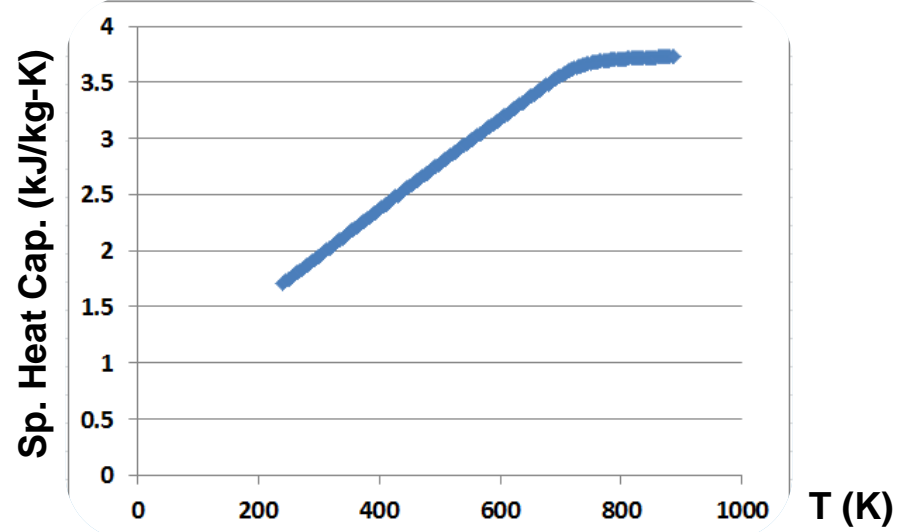
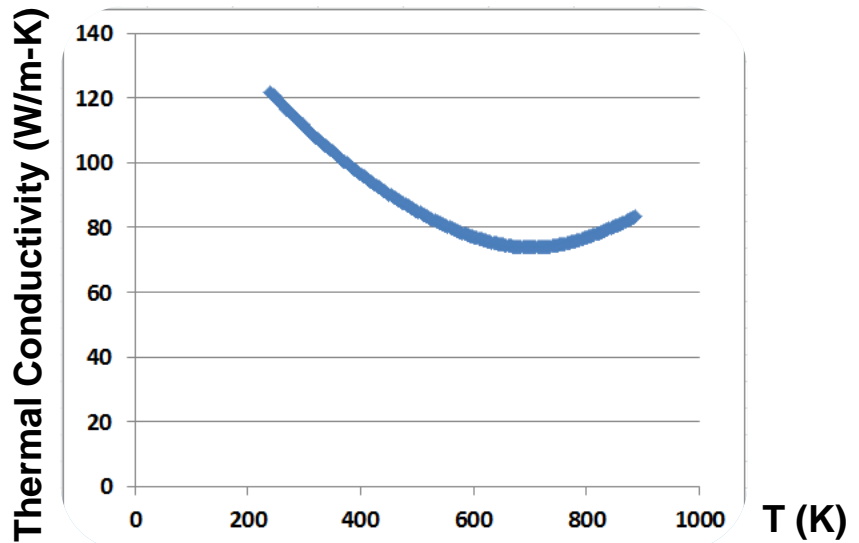
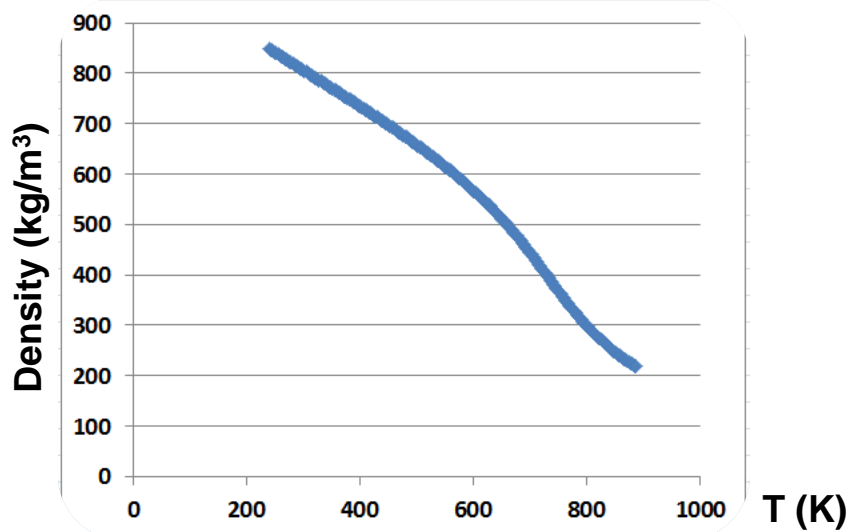
Other Model Particulars



- Model created and simulation performed with Fluent 15
- SST (Shear Strain Transport) k-omega turbulence model with low-Reynolds-number corrections
- Hybrid unstructured (solid) and structured (fluid) mesh with 1.75 million cells
- $y+ = 3$ to 75
- Tube wet (inner) wall surface roughness set to 9 microns
- Perfect thermal and electric contact assumed at all metal-metal interfaces
- Stainless Steel bolts and nuts omitted
- Electric field implemented using User-Defined Scalar Transport and User-Defined Functions



Fluid Properties

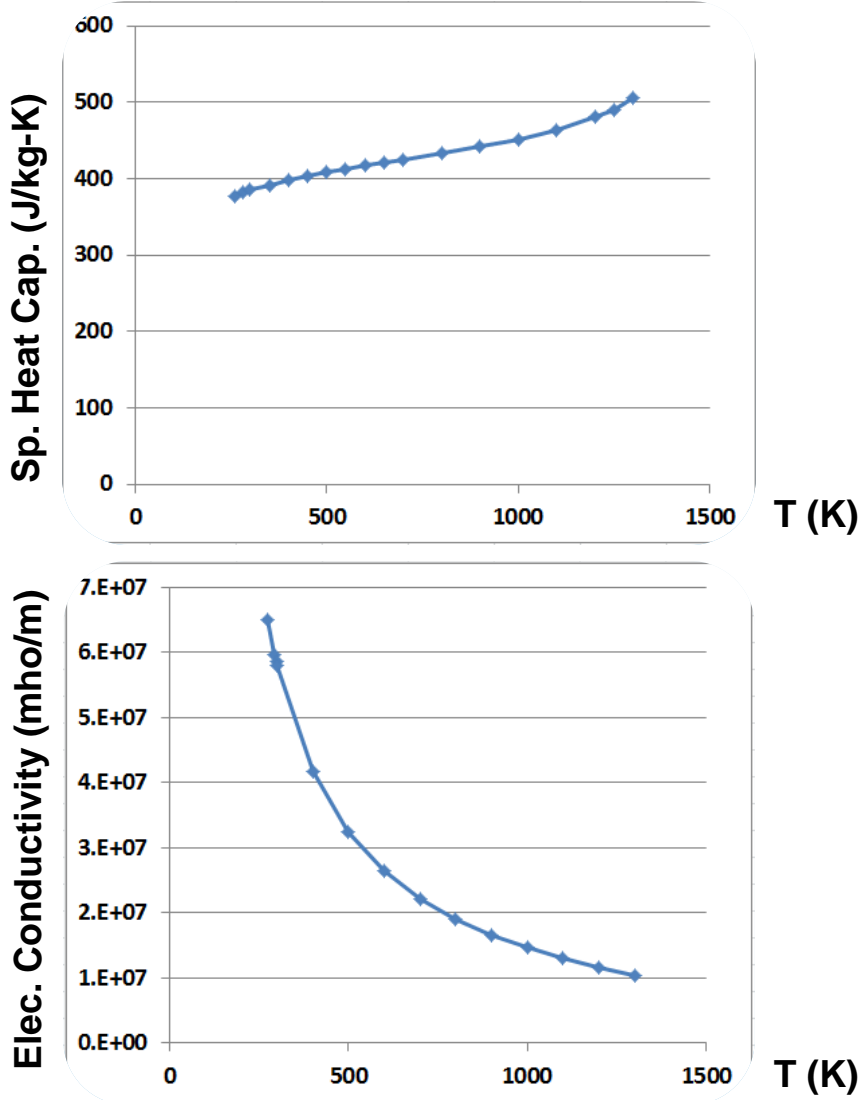
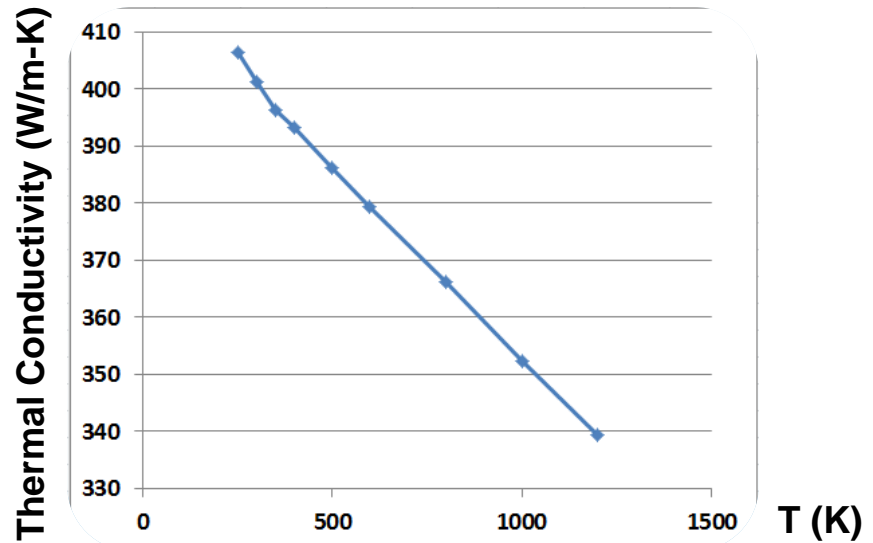




Solid Properties

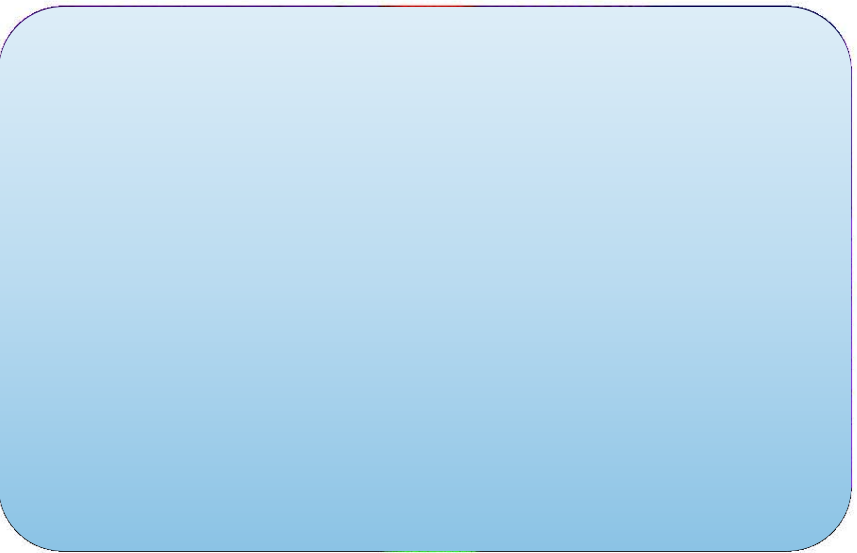
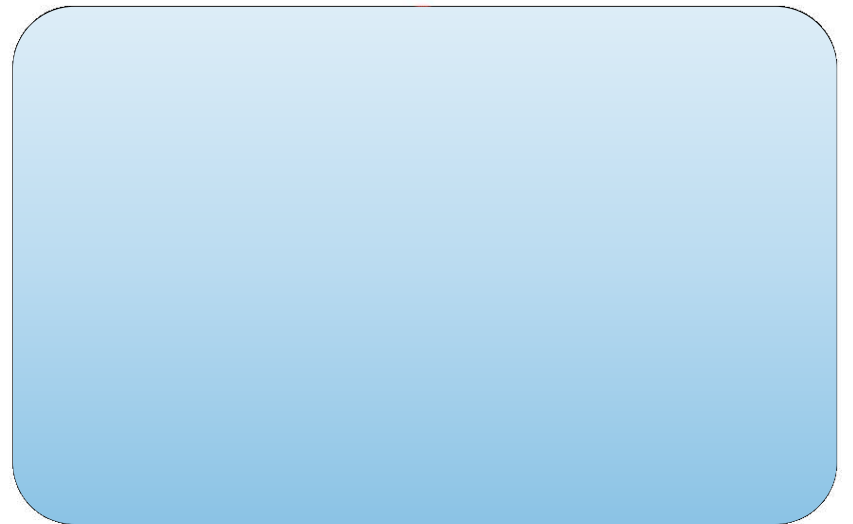


Constant density of Cu
= 8978 kg/m³





Mesh





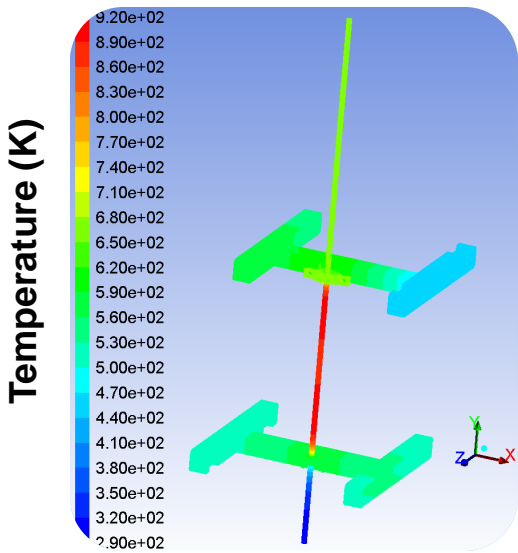
Tube Heat Balance Behavior



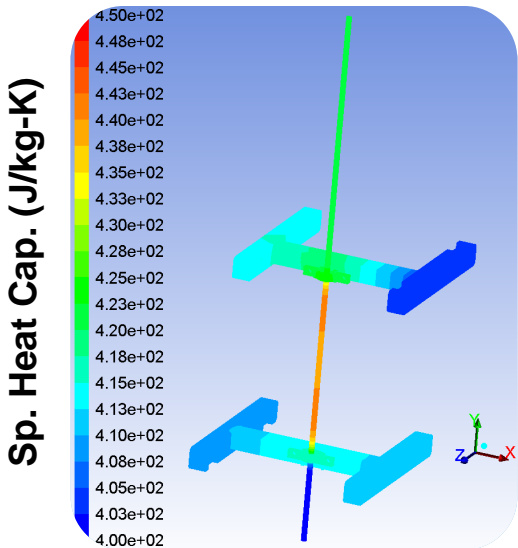
- Main heat rejection from the tube is to the fuel
- Without temperature-dependence of fluid properties, cooling efficacy of fuel is greatly underpredicted
- Model with surface roughness of 1.5 microns (usual value cited for drawn copper) underpredicts the cooling efficacy of the fuel
- For the electric power level used in the experiment, the simulation underpredicts the heat rejected to the fuel, and overpredicts the temperature and resistance of the tube
- Surface roughness was set to 9 microns in the simulation to achieve cooling efficacy similar to experiment



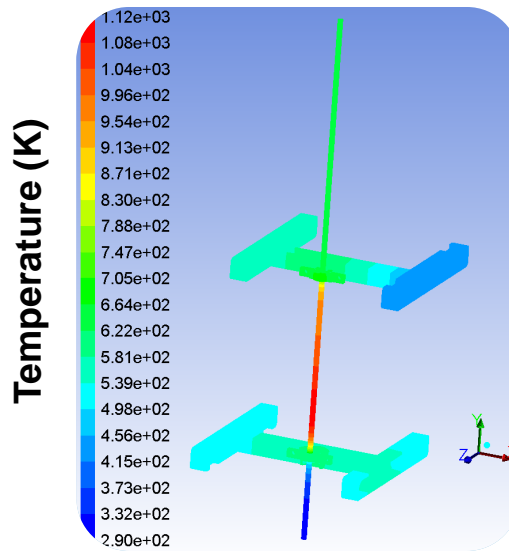
Thermal Variations in Copper



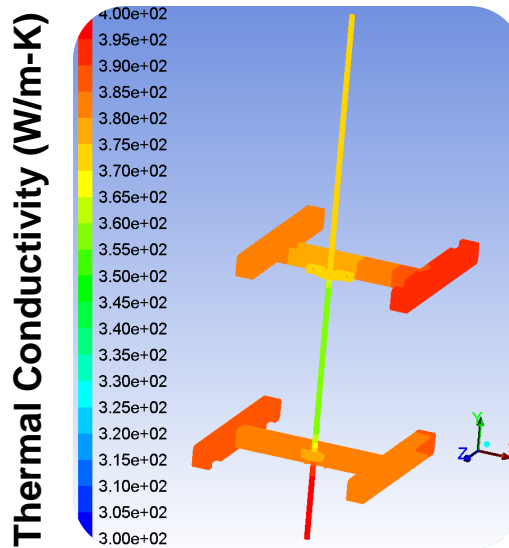
Large temp. spread
~300K to ~900K



Significant thermal
property variations

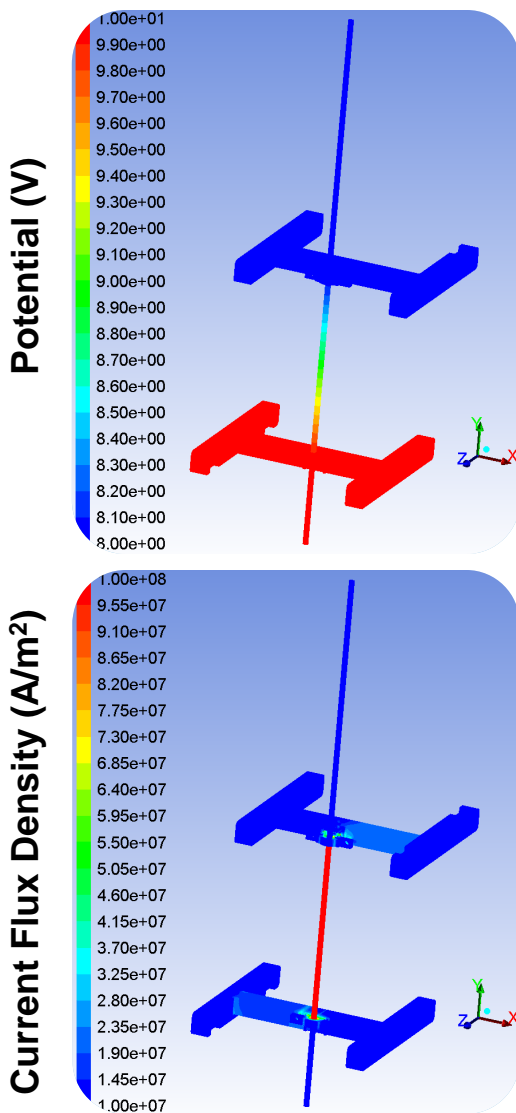


Roughness
1.5 microns
leads to
higher wall
temps. >
1100K



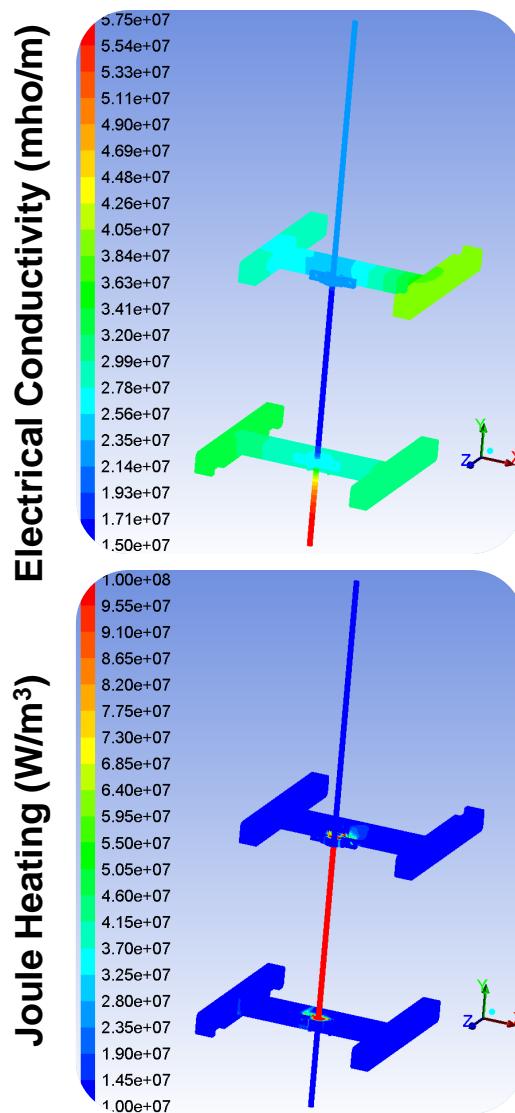


Electrical Field



Almost all the voltage drop is along the tube wall

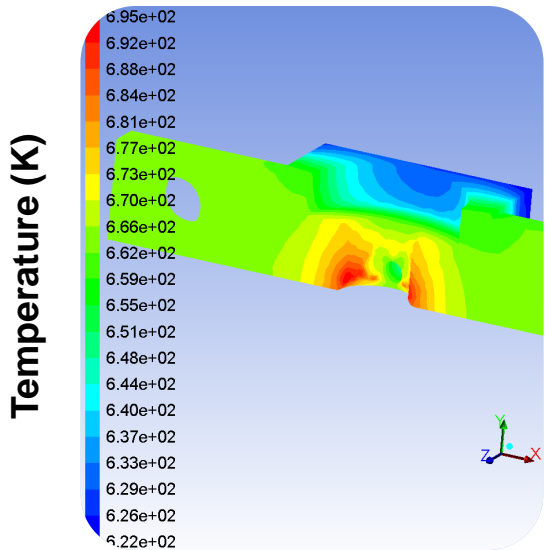
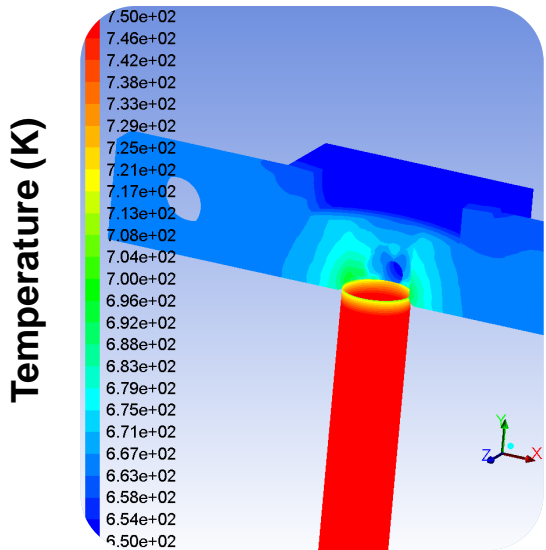
Large thermal changes in elec. conductivity



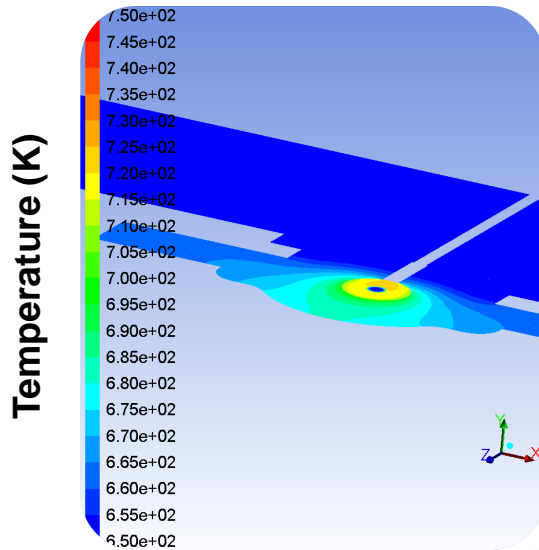
Very large current density and Joule heating in tube wall and at juncture of tube and choke



Temperature Concentration



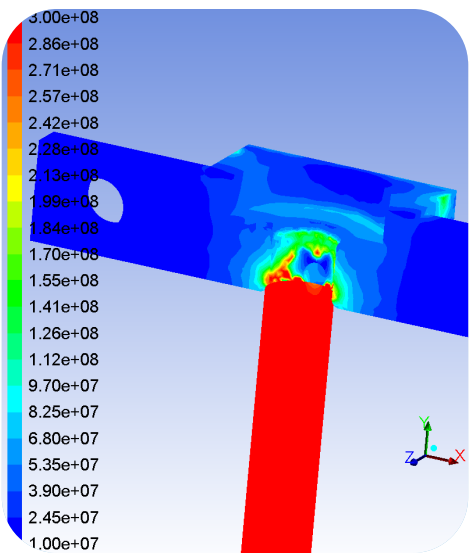
- Large temperature gradients and localized high temperatures occur where tube meets thermal choke
- Seen in two surface temperature views and in $y=6.015625"$ section
- Similar concentration at inlet (bottom) thermal choke



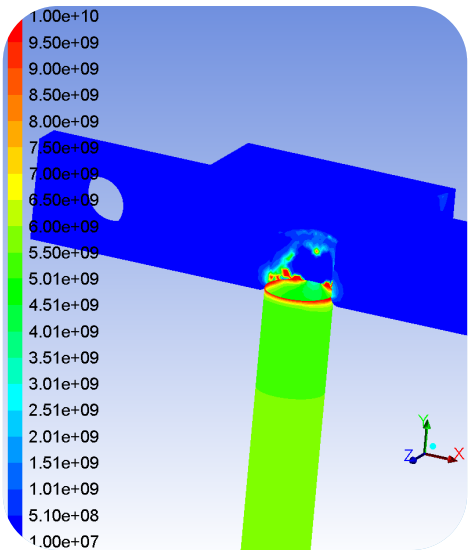


Current Concentration

Current Flux Density (A/m^2)

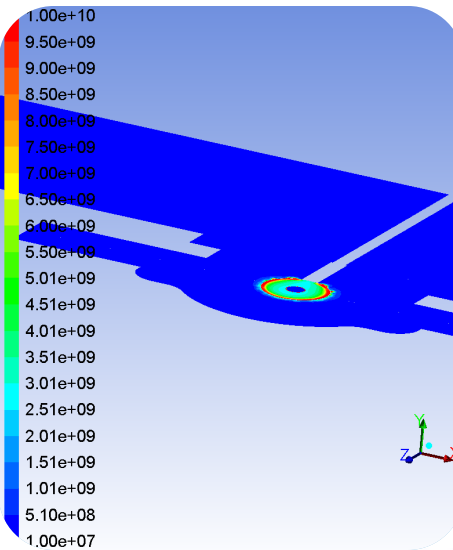


Joule Heating (W/m^3)



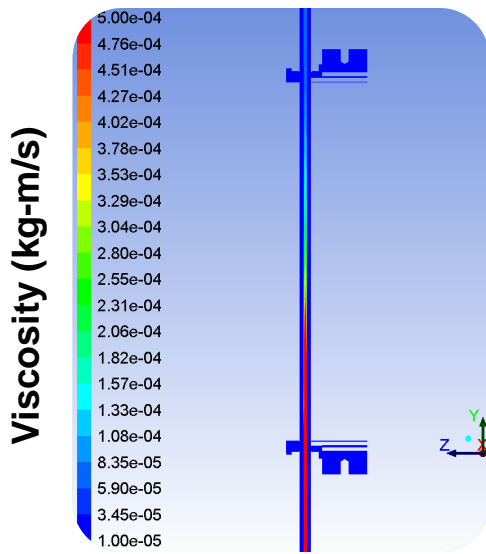
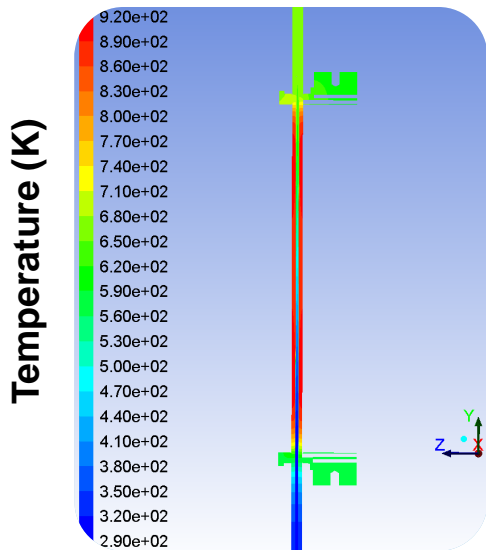
- Current flux density concentration even stronger than temperature
- Current chooses path of least resistance
- Joule heating even more highly localized than current

Joule Heating (W/m^3)

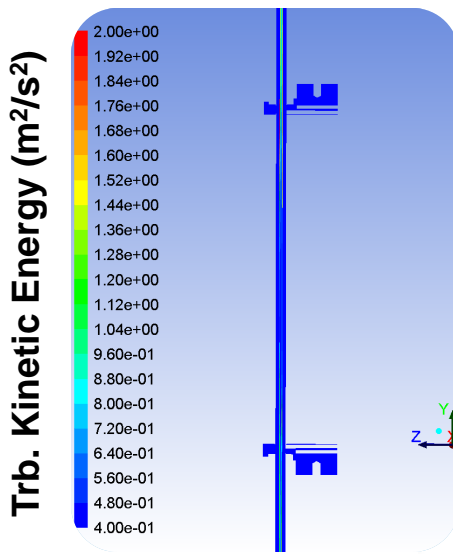




Thermal Variations in RP-2

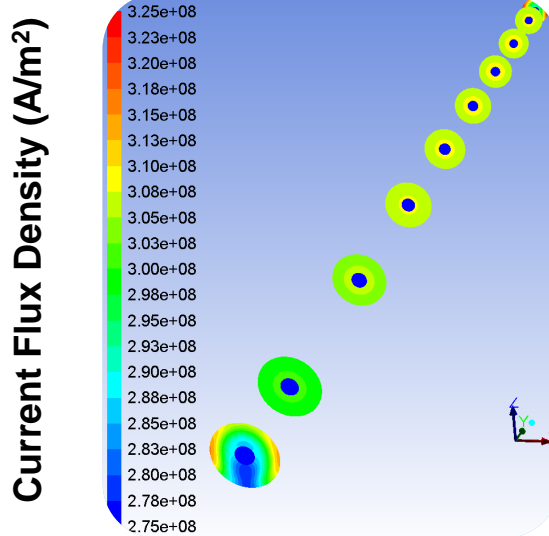
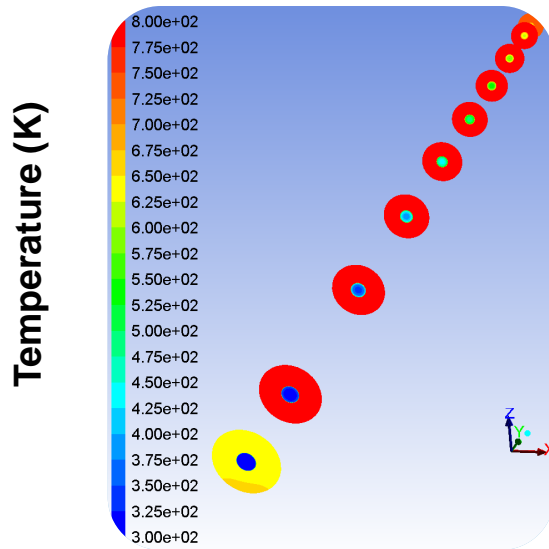


- RP-2 temp. rises from 300K to 660K
- Bulk fluid viscosity is seen to undergo large changes
- Turbulent kinetic energy dips lower in middle stretch of tube due to large gradients in fluid properties

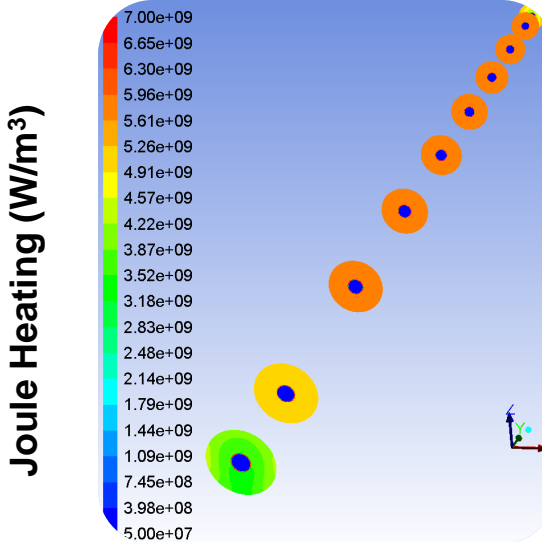




Cross-sections at Thermocouples



- Fluid bulk temperature rise seen in cross-sections at TC locations
- Current flux density seen to be higher at inner tube wall due to lower temperature (path of least resistance)
- Joule heating much higher at inner tube wall





Test Outputs

Steady State
(Average over
three runs and last
100 seconds)

Fuel Outlet Temperature

Back pressure
989 psi

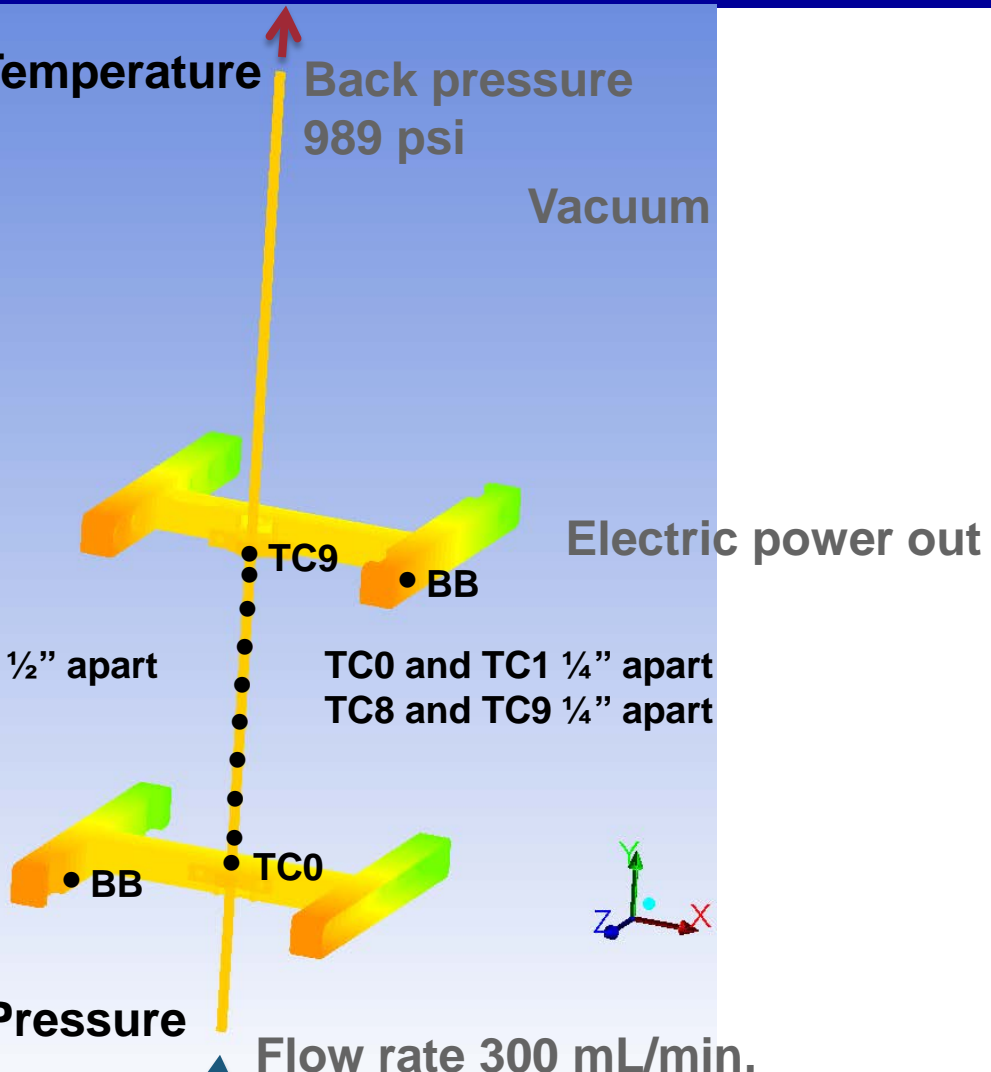
Vacuum

TC1 to TC8 spaced $\frac{1}{2}$ " apart

Electric supply 4400W
Choke-to-choke
Voltage and Current

Fuel Inlet Pressure

Flow rate 300 mL/min,
Temperature 77°F





Experiment vs. Simulation



| Controls | Exit Pressure | Vol. Flowrate | Inlet Temp. | Elec. Power |
|------------|---------------|--------------------|-------------|-------------|
| | MPa | cm ³ /s | K | W |
| Experiment | 6.821688 | 4.9975 | 298.34 | 4415.33 |
| Simulation | 6.821688 | 4.9975 | 298.34 | 4344.44 |

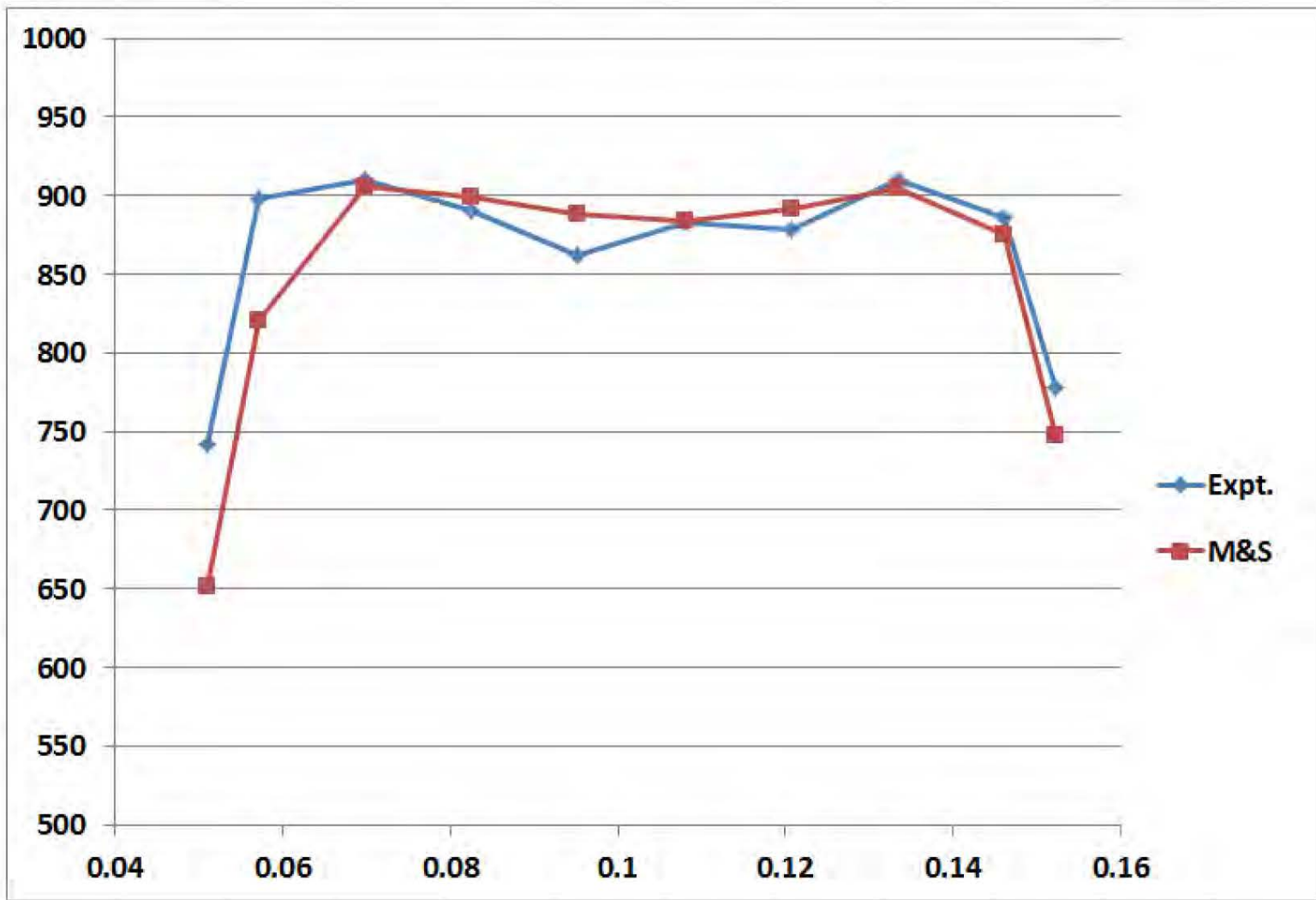
| Output | Volts | Amps | Inlet p MPa | Exit T | Inlet busbar | Exit busbar | Inlet choke | Exit choke | Instr. collar |
|--------|--------|--------|-------------|--------|--------------|-------------|-------------|------------|---------------|
| Expt. | 2.1426 | 2060.7 | N/A | 661.13 | 509.29 | 445.64 | 881.56 | 929.05 | 508.24 |
| Smln. | 2 | 2172.2 | 7.2341 | 659.08 | 509.29 | 445.64 | 576.84 | 639.68 | N/A |

| TC# | 0 | 1 | 2 | 3 | 4 | 5 | 6 | 7 | 8 | 9 |
|-------|-------|-------|-------|-------|-------|-------|-------|-------|-------|-------|
| Expt. | 742.3 | 897.6 | 909.5 | 890.6 | 862.5 | 883.3 | 878.5 | 909.6 | 886.2 | 777.9 |
| Smln. | 651.0 | 820.3 | 905.9 | 899.3 | 888.2 | 884.0 | 891.5 | 905.1 | 875.4 | 747.0 |

All temperatures in K

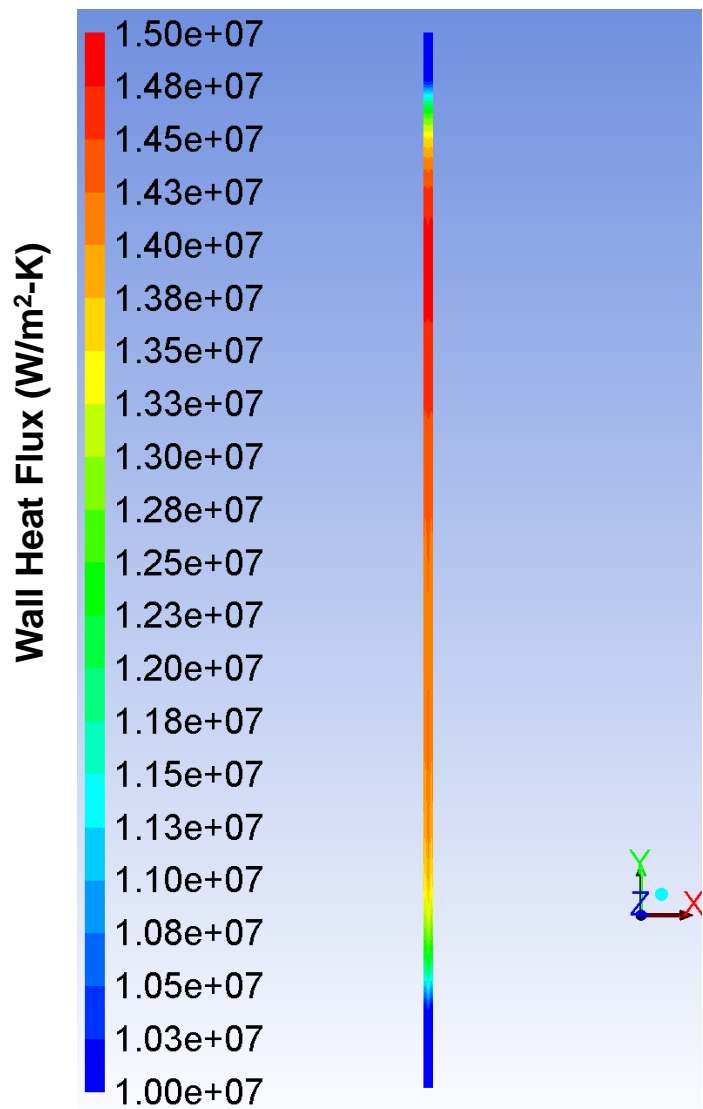
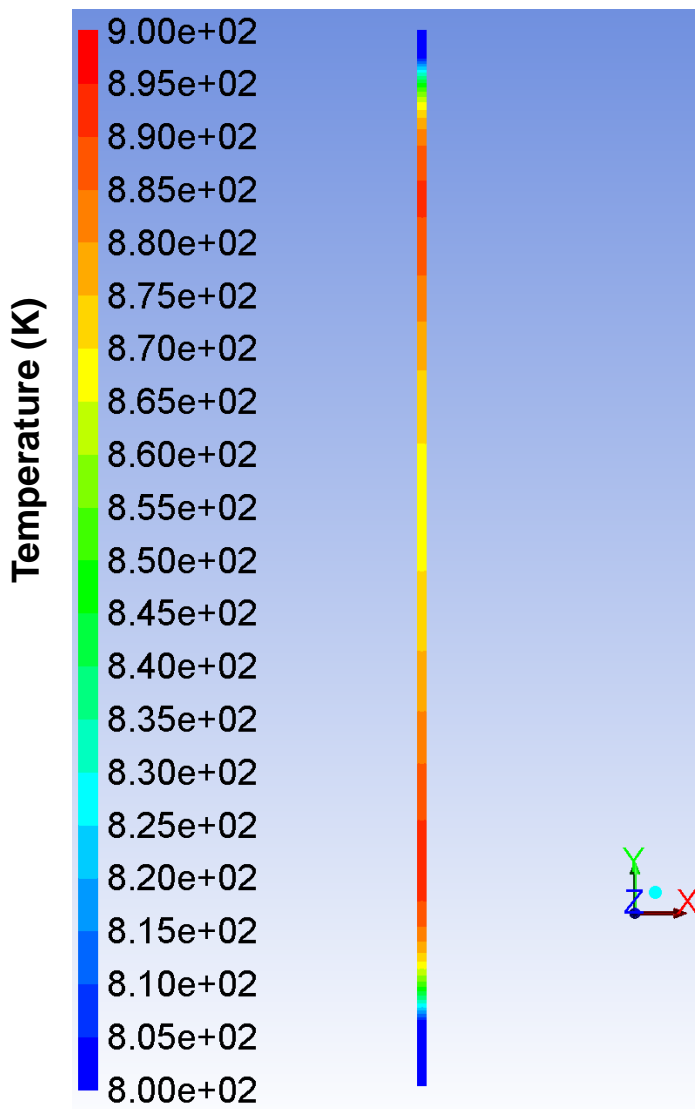


Expt. vs. Simln. – Tube Surface Temps.





Tube Inner Wall Surface





Discussion



- Overall, simulation results seem physically realistic
- Identified location of potentially undesirable current flux and Joule heating concentration
- Two gaps in the model have been identified
 - Model underpredicts cooling efficacy of fuel
 - Possible reasons include uncertainties in surface roughness, fuel properties and turbulence model response to sharp changes in fuel properties
 - Model also underpredicts temperature of both chokes
 - Possible reason is an actual thermal gap resistance at interface of busbar and choke, due to imperfect contact
 - Simulation identified possible failure mode due to overheating of choke or SS bolts



Next Steps



- Refine the mesh to get $y^+ < 1$
- More accurate fluid properties, including pressure-dependence
- Accurate wall surface roughness input
- Cold flow experiment for pressure drop comparison
- Inclusion of SS bolts in analysis
- Thermal/electric contact what-if analysis
- Turbulence model response to sharp changes in fluid properties
- Chemistry and Physics of Insolubles formation and channel fouling



Summary and Conclusions



- Conjugate heat transfer and current flow with RP-2 in an electrically heated tube has been simulated
- Simulation identified Joule heating concentration
- Simulation identified presence of unknown thermal resistance or heat source affecting chokes
- Simulation identified that model physics needs improvement at solid-solid and fluid-solid interfaces
- Lab experiments help identify model assumptions in need of revision and sub-models in need of refinement
- Experiment and Simulation co-evolve to arrive at a validated model and better understanding of physics

